

X-ray holography

V V Lider

DOI: 10.3367/UFNe.0185.201504d.0393

Contents

1. Introduction	365
2. Principles of X-ray holography	366
3. X-ray holography with an external radiation source	367
3.1 In-line holography; 3.2 Off-axis holography; 3.3 Fourier-transform holography	
4. X-ray holography with an external radiation source and a detector (fluorescence holography)	371
4.1 Multiple-energy fluorescence holography; 4.2 Other methods of fluorescence holography; 4.3 Application of X-ray fluorescence holography	
5. Conclusions	380
References	381

Abstract. Different X-ray holography methods are reviewed and their features and capabilities discussed. Particular attention is paid to the fluorescence holography method, which allows obtaining three-dimensional local structure images of ordered objects with atomic resolution. Using concrete examples, it is proved that X-ray holography is a unique nondestructive structural characterization method for a wide class of objects.

Keywords: holography, X-rays, coherency, fluorescence, atomic resolution

1. Introduction

Holography is a branch of science and technology whose object of study is the procedure of recording and subsequently reconstructing the information about an object, contained in physically realizable or mathematically described wave fields, with the use of wave diffraction and interference, including the solution of technological problems related to the use of this information.

The idea of the holographic method was formulated by the English physicist Gabor in 1948 [1]. Also at that time Gabor introduced the term hologram [derived from Greek holo (complete) and gram (notation)].

The basics of holography were formulated in the 1950s and the early 1960s. For instance, Rogers [2] made a significant contribution to holography by obtaining the first phase holography and elaborating the theory; in 1963, Van der Lugt showed in [3] that phase information might be

encoded in the interference fringes of a diffraction pattern.

The first holographic experiments were carried out using visible light sources. Unfortunately, suitable coherent light sources required for demonstrating all holography capabilities were nonexistent at that time, and only modest results would support this idea for many years. In 1963, Leith and Upatniek [4] applied a laser to holography, and the results obtained by Stroke, Leith, and their collaborators [5–7] lent an impetus to the rapid development of holography.

Because of their shorter wavelength, X-rays provide a way to obtain a higher resolution than that for visible light. X-ray holography was proposed by Baez [8] in 1952, several years after the invention of holography by Gabor. Leith, Stroke, Winthrop, et al. [9–13] laid the theoretical foundations of high-resolution X-ray holography. No significant progress was made until Aoki and Kikuta [14] and Reuter and Mahr [15] recorded and reconstructed an X-ray hologram with a resolution of several micrometers.

However, progress was slow, because there was still no sufficiently bright X-ray radiation sources to provide a beam of sufficient coherence required to observe a hologram with high resolution. The situation changed radically with the advent of high-brightness radiation sources based on synchrotron radiation (SR) storage rings and the first X-ray free-electron lasers (FELs). It became evident that synchrotron sources are capable of providing the requisite beam coherence [16] and that short-pulse lasers hold promise for their application in the near future [17].

The methods of structure analysis that use X-rays, for instance, X-ray diffractometry, have found wide use in studies of crystal structure. However, the determination of atomic positions with these methods is not unambiguous. Therefore, a demand has arisen for a technique of direct three-dimensional (3D) atomic imaging to aid in determining the crystal structure of the object under investigation.

Although the emergence of atomic-resolution X-ray holography was expected, its experimental implementation became possible only after the publication of Szöke's paper [18], which established theoretically that fluorescence X-rays and photoelectrons of ionized atoms of a crystal under

V V Lider Shubnikov Institute of Crystallography,
Russian Academy of Sciences,
Leninskii prosp. 59, 119333 Moscow, Russian Federation
Tel. +7 (499) 135 61 50
E-mail: lider@ns.crys.ras.ru; vallider@yandex.ru

Received 26 November 2014, revised 23 February 2015
Uspekhi Fizicheskikh Nauk **185** (4) 393–413 (2015)
DOI: 10.3367/UFNe.0185.201504d.0393
Translated by E N Ragozin; edited by A M Semikhatov

investigation, which are radiation sources, might form an atomic-resolution hologram.

The first holograms were formed using electrons [19–21]. However, electrons are not a perfect means for holographic visualization owing to their strong interaction with substances and large phase shifts in scattering. These factors are responsible for hologram distortions. But phase shift and multiple scattering effects are negligible for X-ray radiation. Furthermore, the advantage of X-rays consists in their higher penetrability. That is why the use of X-rays for the experimental realization of fluorescence holography is preferred over the use of electrons.

Although the main idea of the method was expressed in 1986 and the results of numerical simulation of a fluorescence hologram were published in 1991 [22], it was experimentally implemented using X-rays only 10 years later [23].

The X-ray holography methods can be conventionally divided into two classes: methods that rely on Gabor's idea and use an external radiation source and detector, and methods that use an internal radiation source (detector). There are several reviews [24–30] concerned with the latter class of methods and only one (!) review [31] concerned with the former. In the majority of these reviews, there is a comprehensive description of the main features of X-ray holography and the physical processes participating in hologram formation. Some of the reviews describe the methods and progress achieved with their aid over certain periods [24–26]; others, published relatively recently [28–30], place primary emphasis on a detailed analysis of determinative theoretical and experimental achievements, passing over those believed by the authors to be less significant.

The objective of this review is to describe the features of all known methods of X-ray holography.

2. Principles of X-ray holography

The central idea of Gabor's method can be illustrated by the example of using visible light. The principle applies to the radiation of arbitrary energy, to X-ray radiation in our case (the term X-rays is commonly used in reference to electromagnetic radiation with wavelengths ranging from 10 nm to 10^{-3} nm, which corresponds to a photon energy range between 100 eV to 1 MeV; there are no commonly accepted boundaries with UV radiation in the soft region and with gamma-ray radiation in the hard one).

To be suitable for holography, X-ray radiation must be monochromatic with a relatively high degree of coherence, which permits two waves — the reference wave and the object wave (i.e., the wave reflected by the object of investigation) — to interfere constructively or destructively [32]. The so-called longitudinal (temporal) coherence can be characterized by the effective finite length of a wave train. Two overlapping trains produce a pattern of interference fringes or merely an incoherent background, depending on the degree of their overlap and the constancy of their phases. As a rule, a detector should be spaced at a distance d from a sample of size a such that the Fraunhofer condition

$$a^2 \ll d\lambda \quad (1)$$

hold, where λ is the radiation wavelength.

Holography involves two steps.

Step one: hologram recording. The recording of the interference pattern arising in the mixing of the reference

wave with the wave scattered by the object. When the reference and object waves meet in space, a system of standing waves forms with maxima corresponding to zones in which the interfering waves are in phase, and with minima in which the waves are in antiphase. The image in the hologram bears some resemblance to the object, but diffraction effects can make it much more complex.

From two measured intensity patterns (with and without an object), it is possible to calculate the hologram contrast [31, 33–36]

$$I(\mathbf{r}) = |A(\mathbf{r}) + R(\mathbf{r})|^2 - |A(\mathbf{r})|^2 \\ = |R(\mathbf{r})|^2 + A(\mathbf{r})R^*(\mathbf{r}) + A^*(\mathbf{r})R(\mathbf{r}), \quad (2)$$

where $A(\mathbf{r})$ and $R(\mathbf{r})$ are the respective complex amplitudes of the object and reference waves, \mathbf{r} is the vector that defines a point in the detector plane, and the symbol * denotes complex conjugation. The hologram intensity pattern bears information about the object (the term $A(\mathbf{r})R^*(\mathbf{r})$) as well as about the virtual twin (the complex conjugate term $A^*(\mathbf{r})R(\mathbf{r})$); the terms $|R(\mathbf{r})|^2$ and $|A(\mathbf{r})|^2$ respectively describe the reference and object wave intensities.

Step two: image reconstruction. Using the interference terms $A(\mathbf{r})R^*(\mathbf{r})$ and $A^*(\mathbf{r})R(\mathbf{r})$, the image of the object can be reconstructed, for instance, by using the Kirchhoff–Helmholtz transformation [36–39]

$$K(\mathbf{r}) = \int_S I(\xi) \exp\left(\frac{2\pi i \xi \mathbf{r}}{\lambda \xi}\right) dS \quad (3)$$

and the Fourier analysis [40, 41].

Integration in expression (3) is performed over the screen surface S with coordinates $\xi = (X, Y, L)$, where L is the distance of the source from the screen center (the detector plane). The function $K(\mathbf{r})$ is significantly structured and nonzero only in the spatial domain occupied by the object. A 3D image can be constructed from one 2D hologram by reconstructing the wavefront $K(\mathbf{r})$ for several planes located in the immediate vicinity of the object at different distances from the source.

Owing to the presence of two interference terms in expression (2), reconstruction gives rise to real and virtual object images [37] recorded in three dimensions.

The following advantages of holography can be highlighted [42]:

(1) it is less prone to the loss of resolution than other X-ray methods;

(2) it provides a greater depth of focus and thereby permits obtaining the amount of information in one exposure that requires several exposures with other methods;

(3) it obviates the need for optical devices that are difficult to make for application in the X-ray wavelength range.

Reconstructing the image of an object permits viewing it in every detail, including its volume contour, parallax, and depth-of-focus effects. Furthermore, the two-step nature of holography opens up the extraordinary possibility of *a posteriori* processing (upon conclusion of the experiment) of the information contained in the scattered wave. This implies the possibility of performing filtration, spectral selection, and aberration correction, removing imaging artifacts, and, lastly, changing the point of observation. It is difficult to fully appreciate the possibilities offered by this new technique of physical experiments [43].

3. X-ray holography with an external radiation source

3.1 In-line holography

In Gabor's original scheme, a single light beam was used, whose light passed by the object of investigation serving as a reference wave. In the illumination of an object by a plane coherent wave, the hologram consists of contrasting concentric circles (Fig. 1). The radius r_n of the n th ring is expressed as $r_n = (2nd\lambda)^{1/2}$, where d is the distance between the object and the hologram plane.

The resolution δ is limited by the numerical aperture NA: $\delta \geq \lambda/2 \text{ NA}$ [35, 44]. The quantity NA is defined by the maximal angle at which the interference fringes are recorded with good visibility. The conditions whereby the radiation source size s and the detector 'grain' size blur the interference fringes determine the spatial resolution of in-line holography [8, 14]:

$$\delta = \left\{ \left(\frac{0.61\sigma}{M} \right)^2 + \left[\frac{1.22s(M-1)}{M} \right]^2 \right\}^{1/2}. \quad (4)$$

Here, σ is the detector resolution and M is the magnification defined by the ratio of the source-detector and source-object distances. In the limit cases of a plane reference wave ($M = 1$) and a spherical reference wave ($M \gg 1$), it follows from formula (4) that the resolution is determined only by the detector resolution ($\delta = 0.61\sigma$) or only by the source size ($\delta \approx 1.22s$), respectively.

The use of a spherical wave as a reference one offers several advantages. First, due to the magnification of an interference pattern, the detection resolution is determined by

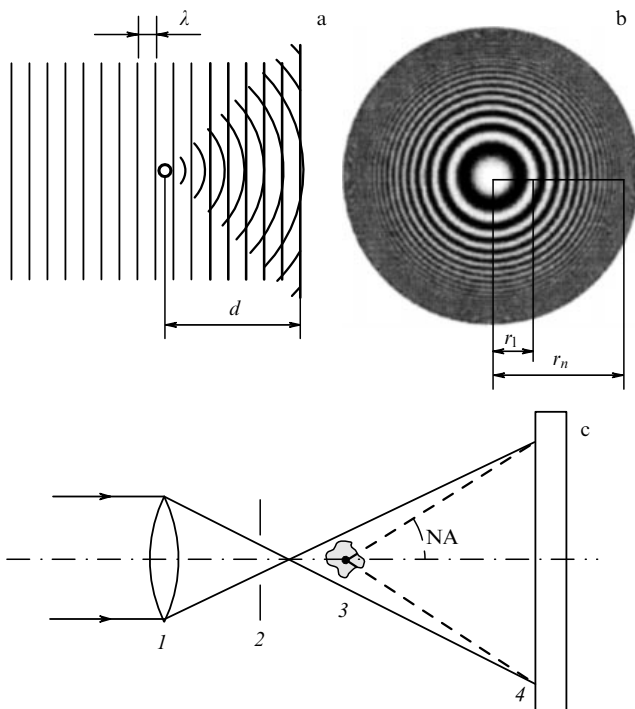


Figure 1. (a) In-line holography schematic and (b) hologram obtained in the illumination of the research object by a plane wave. (c) Schematic of on-axis holography in the illumination of an object by a spherical wave: 1—focusing optics, 2—order sorting aperture, 3—the object, 4—detector, NA—numerical aperture.

the ratio σ/M , which is important for overcoming the resolution limit imposed, for instance, by the pixel size of a CCD detector, frequently employed in in-line digital holography. Second, by placing the X-ray beam focus in the immediate vicinity of the object under investigation, it is possible to increase the object beam intensity to a level comparable to the reference beam intensity and thereby improve the hologram contrast [44].

In the soft X-ray range, a spherical wave can be produced by focusing the primary X-ray beam with the use of spherical multilayer mirrors [45], Fresnel zone plates [46–50], or radiation filtration with a small-radius aperture stop (pin-hole) [51–53]. Experiments have shown the feasibility of attaining a resolution of at least 1 μm , which is limited primarily by small numerical apertures.

Figure 2 shows the results of investigations of dried siliceous diatoms using radiation with an energy of 250 eV [49]. In this case, it was possible to attain a spatial resolution of $326 \pm 90 \text{ nm}$. The use of a photoresistor as the X-ray detector and a scanning atomic force microscope for the subsequent data reading permitted improving the resolution to 40–60 nm [54–57].

The use of Fresnel-zone plates may offer a major practical advantage in FEL-assisted investigations, because it permits using the entire FEL beam width and thus opens the way to single-pulse in-line digital holography with radiation of femtosecond duration. However, the realization of this advantage is hindered by the emergence of three main drawbacks. First, the alignment of optical elements is a more complex task than the alignment of a pinhole. Second, the zone plate may be damaged, if not destroyed, by an FEL pulse. And third, more stringent requirements for the coherence of the radiation source emerge because the zone plate collects a greater part of the beam than the part collected by a pinhole [48, 49].

Fresnel-zone plates are also used to advantage for focusing hard X-ray radiation. For instance, the use of X-ray undulator radiation and a high-resolution zone plate permitted the authors of Ref. [58] to obtain a focus 0.1–0.3 μm in size in the wavelength range 0.45–1.5 \AA . The authors of Ref. [58] reported the possibility of forming a diverging X-ray beam at a wavelength of 1.127 \AA for a virtual source size of 200 nm using two 'crossed' planar waveguides.

Owing to the simplicity of hologram alignment and recording, in-line holography is widely used in various applications, for instance, in investigating biological objects [48, 49, 52–55] and magnetic structures [60]. The main

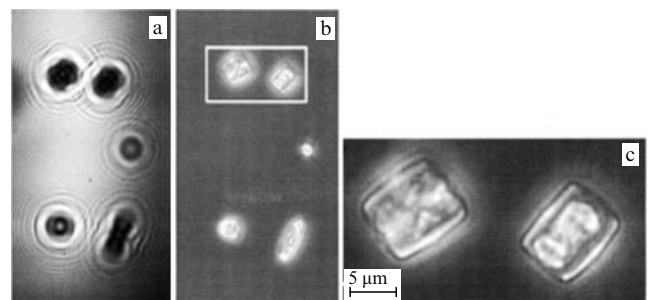


Figure 2. (a) Hologram of dried diatoms *N. perminuta* obtained with the use of X-rays with an energy of 250 eV, which were focused with a zone plate. (b) Reconstruction of the hologram shown in Fig. 2a. (c) Magnified image of the part enclosed in the rectangle in Fig. 2b.

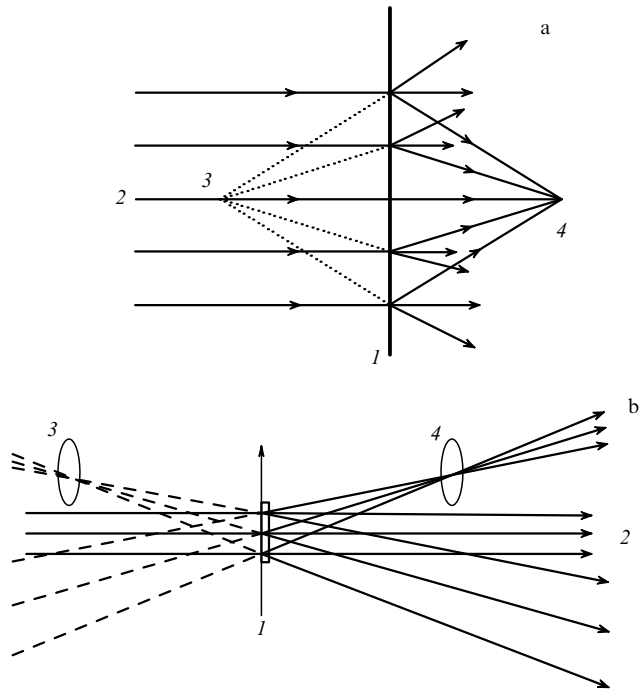


Figure 3. Double-image formation schematics in the cases of (a) in-line and (b) off-axis holography; 1—hologram, 2—coherent reconstruction beam, 3—virtual (twin) image, 4—real image.

limitation of in-line holography is the so-called double image effect, which emerges as follows [57].

If it is assumed that image reconstruction is effected using the initial reference wave, the reconstructed image intensity is equally divided between diffraction orders $+1$ and -1 in such a way that two images are formed: the first, virtual, at the location of the sample and the second, real, on the other side of the hologram (Fig. 3a). In the real image plane, the diverging beam from the virtual image interferes with the nondiffracted beam (the zeroth-order beam). As a result, the second hologram forms at twice the distance from the object, which is superimposed on the real image. The signal due to the second hologram bears information that distorts the real image. This distortion can be small only when the far-field condition is fulfilled [see formula (1)]. Otherwise, the virtual ('twin') image may be eliminated using an iterative procedure [33, 38, 44, 59, 61–64], which primarily involves forward and backward field propagation between the screen and the object plane until all artefacts associated with the double image disappear. However, even in this case, in Gabor's opinion [65], the separation would never be complete: in the field of coherent illumination, each point produces a wake perturbation behind itself, which extends over a long distance.

3.2 Off-axis holography

In the configuration of in-line holography, three constituent parts of the reconstructed image—the zero diffraction order and two conjugate images, virtual and real—are superimposed on each other and cannot be observed separately. In the off-axis geometry proposed by Leith and Upatniek [4], these image parts propagate in different directions and can be observed separately (Fig. 3b).

In off-axis holography, one of the two beams 'works' as a reference wave and the other illuminates the sample at an angle $\Delta\theta$ (Fig. 4a). In this method, the sample size a must be

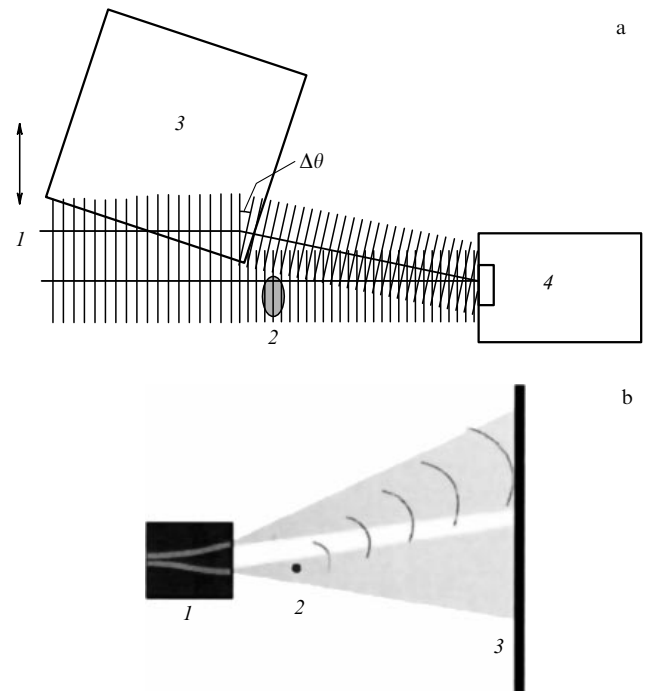


Figure 4. Experimental setups of off-axis holography. (a) Experiment scheme using a prism as a splitter [66]: 1—primary beam, 2—sample, 3—scanning prism, 4—detector. (b) Experiment scheme using a waveguide [70]: 1—waveguide, 2—sample, 3—detector.

smaller than the transverse coherence length and must satisfy the condition $a < d\Delta\theta$ [66].

Off-axis holography solves the problem of image overlap, but requires an additional optical element (a mirror or a prism [67]) and a wide coherent beam, which may be a problem in the operation with radiation in the X-ray range. Nevertheless, off-axis holography was first demonstrated in the hard X-ray range with the use of a prism splitter (beam splitter) [66].

The complex amplitudes in the detector plane were determined by the method of interference fringe scanning quite often used in X-ray interferometry [68, 69]. For the interference fringe spacing $\Delta r \approx 2.6 \mu\text{m}$ ($\Delta r = \lambda/\Delta\theta$), it was possible to obtain the images of phase objects about $6 \mu\text{m}$ in size.

To obtain X-ray off-axis holograms in Ref. [70], two mutually coherent conical beams emanating from a pair of X-ray channel waveguides were used (Fig. 4b). A magnified off-axis hologram lends itself to quick and precise reconstruction. The waveguide lengths in the scheme presented can be adjusted in order to completely reject the background radiation, even for X-ray photons of high energy. In this case, the spatial resolution is limited by the size of the waveguide cross section. For curved waveguides, the spacing of the two beams can be comparable to the transverse coherence length of the primary beam.

3.3 Fourier-transform holography

Fourier-transform holography is a version of off-axis holography, in which the reference wave source (the reference) is located in the plane of the object itself; this plane is perpendicular to the primary beam direction and parallel to the recording plane (Fig. 5a). In this case, the amplitude–phase relations between the object wave in the hologram plane and the object plane are mathematically expressed as the Fourier transformation. Consequently, the object can be

numerically reconstructed using the inverse Fourier transformation of the squared intensity modulus of the interference pattern recorded by the detector. This simple reconstruction technique permits a rapid reconstruction of the object image using a digitized hologram.

To provide phase matching, a common source is used to illuminate the sample and the reference. The sample object and the reference should be illuminated such that the transverse coherence length exceeds the spacing between them. In the most general case of the Fourier-transform holography implementation, the reference wave has its origin in a small-diameter opening in an X-ray-opaque metallic foil (mask) located in the immediate vicinity of the object [71–74]. In this case, when the distance d between the source and the recording plane is much greater than the distance x between the reference and the object, the interference pattern consists of linear fringes uniformly spaced at $\lambda d/x$, as shown in Fig. 5b.

The main advantage of the method under discussion over other X-ray microscopy methods is the large spacing of the interference fringes on the hologram and, consequently, loose requirements for the spatial detector resolution. Since the geometry of the method allows recording data for large scattering angles, the resolution is typically limited by the spatial extent of the reference.

Figure 6a shows the hologram of a siliceous diatom [74]. A mask with a reference 450 nm in diameter located at a distance of 65 μm from the object window 33.5 μm in diameter was used. The photon energy of the primary beam was equal to 150 eV. The hologram was reconstructed (Fig. 6b) with a resolution of 450 ± 30 nm, which corresponds to the reference size. The skeleton of the diatom structure is clearly seen.

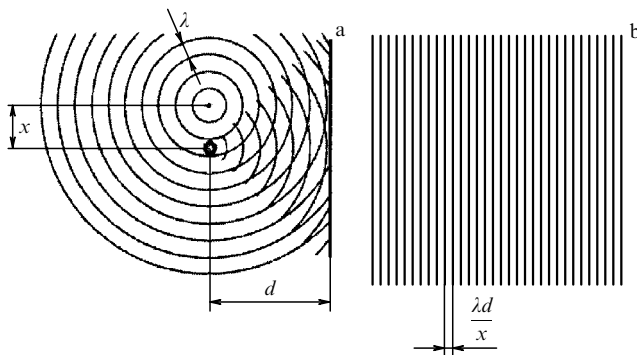


Figure 5. Schematic of (a) Fourier-transform holography and (b) hologram form.

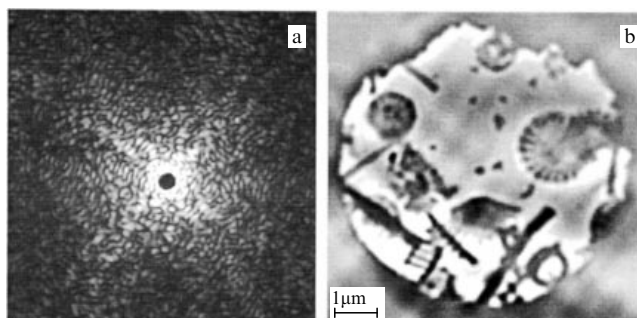


Figure 6. (a) Hologram of a siliceous diatom and (b) its reconstruction [74].

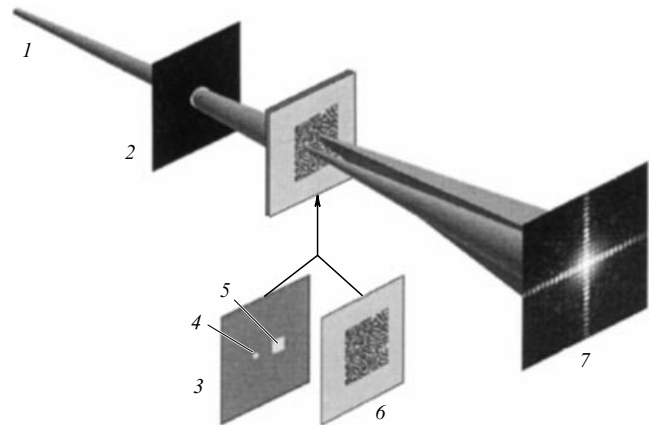


Figure 7. Schematic of scanning Fourier-transform holography: 1—primary X-ray beam, 2—pinhole, 3—mask containing a reference hole 4 and the illumination window 5, 6—sample, 7—detector [77].

X-ray Fourier-transform scanning holography for soft and hard X-ray ranges was developed in Refs [75–77]. The holographic mask containing the reference (Fig. 7), a small-size object window, and the object holder are separated, but are in contact with each other. In this configuration, the sample region under study is varied by translation relative to the mask. The field of view can thereby be increased in the course of experiment.

A drawback of a small opening (a pinhole) that generates the reference wave is the competition between spatial resolution and reconstruction contrast, because the image contrast is defined by the X-ray photon flux in the reference beam. The hologram contrast depends on the relative amplitudes of interfering wave fields and is highest when these amplitudes are equal. With decreasing the reference diameter, the resolution limit decreases linearly, while the reference signal intensity and eventually the image contrast decrease quadratically. Therefore, the conditions of a high-resolution experiment are usually determined by a balance between the desired resolution and the requisite magnitude of the reference signal.

Several ways of increasing the reference wave intensity are described in the literature.

1. *Increasing the number of references.* In this case, an odd number of references is arranged around the sample [78–83]. This increases the number of reconstructed images and, accordingly, the signal-to-noise ratio increase owing to the averaging of the images. Nevertheless, too many references may result in the overlap of the images; that is why their maximal number, in the view of the authors of Ref. [79], is practically limited to five.

As shown in Fig. 8a, in the experiment in Ref. [78], the holographic mask contains the letter F, which plays the role of an object. Its surrounding five openings provide a multiplicity of reference wave sources. The mutual opening–source correlation produces two images: the real image and its complex conjugate, imaginary one (Fig. 8b). In Refs [80–82], five references were also used.

However, more complex reference configurations are also possible. For instance, in Ref. [84] the object was surrounded by twelve openings (each 2.5 μm in diameter) arranged in groups of three on four circumferences of the radii 170, 294, 382, and 512 μm .

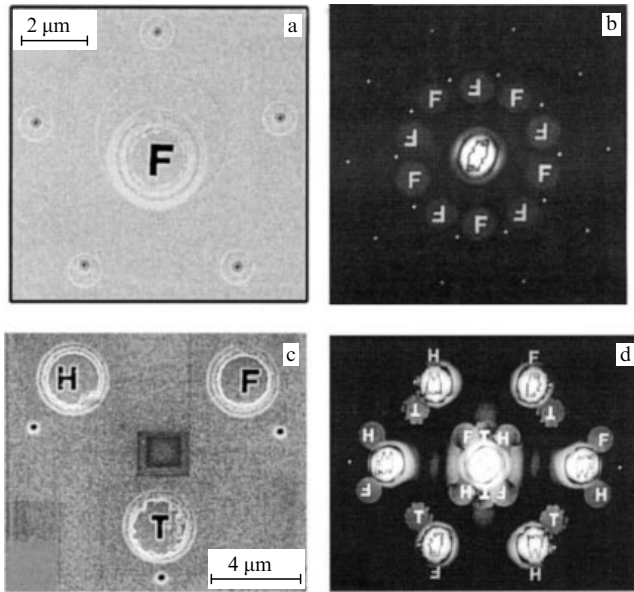


Figure 8. (a, c) Mask and (b, d) reconstructed holographic images for an object (letter F) with five references arranged around it [78] (a, b) and several objects (H, F, T) with their own references [85] (c, d).

It was shown in Refs [85–87] that several objects and reference waves are capable of widening the effective field of view of the method. It is noteworthy that separate objects can be imaged simultaneously (Figs 8c and 8d) without sacrificing spatial resolution. Since every object has its own reference attached, it becomes possible to improve the visibility (contrast) of the interference pattern. The experiment geometry is applicable for ultra-fast imaging, which is especially topical for experiments on an FEL.

2. Reference geometry. The idea of using a slit in the form of a right angle, which determines the field of view and serves as the holographic source of a reference wave, was first proposed in [88]. This method was generalized by the authors of Ref. [88] in the framework of holography with extended reference by autocorrelation linear differential operation (HERALDO). HERALDO is an off-axis holographic method in which the reference wave is formed by a sharp boundary or edge. It permits using a large-size reference with retention of a high resolution. In principle, the high resolution in this case is no longer limited by the reference size; rather, it depends on the quality and sharpness of the constituents. The solution to the problem of improving hologram contrast is facilitated in this case because the flux formed by an extended reference may be much higher than the flux produced by a small-size opening. Furthermore, making extended objects turns out to be less demanding in terms of precision, and slots can be made narrower than the diameter of the opening [90].

It was experimentally shown in [91, 92] that the method under discussion provides a high spatial resolution as well as the possibility of obtaining a hologram with nanodimensional resolution for a single sample exposure to a femtosecond pulse [93].

Figure 9 is intended to demonstrate the advantages of a right-angle shaped reference over a round opening by the example of an object reminiscent of a square slice of cheese.

The method of Fourier-transform holography was enhanced with the help of a specially developed reference pattern termed a ‘uniformly redundant array’, which sub-

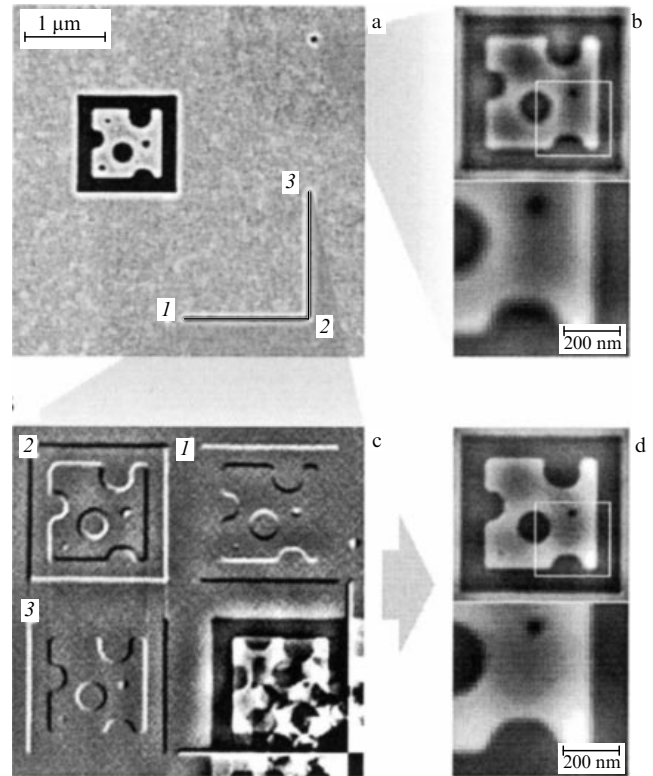


Figure 9. Reconstruction of a ‘cheese’-like sample. (a) General mask form. (b) Reconstruction of a Fourier-transform hologram with the use of a round opening as the RO and a magnified image of the lower right part of the sample. (c) Three relief images of the sample obtained using an RO in the form of a right angle. (d) Reconstruction of the hologram depicted in Fig. 9c by the HERALDO method and a magnified image of the lower right part of the sample enclosed in a white square contour [92].

stantially increases the signal intensity in comparison with that from a single reference beam source without sacrificing resolution. It is significant that the gain in photon flux relative to the single-opening flux is due to the active pattern elements, numbering 162 in the experiments in Ref. [94].

3. Use of Fresnel-zone plates. To increase the reference wave power, the authors of Ref. [95] proposed the use of Fresnel-zone plates. In this case, the first diffraction order of a zone plate, 2 (Fig. 10a), is used to produce a spherical reference wave, while the nondiffracted primary beam (the zeroth order) serves to directly illuminate an object, 4 [96–100]. The function of an order sorting aperture, 3, which is located near the mask with the object, is to reject the higher diffraction orders produced by the zone plate. Owing to a high intensity of the reference wave, this method permits overcoming the size limitation of the object with retention of nanodimensional resolution. The spatial resolution is then limited by the size of the focal spot formed by the zone plate. The in-focus X-ray photon flux, i.e., the intensity that defines the image reconstruction contrast, is proportional to the diameter of the zone plate, while the focal spot size is determined by the width of its outer zone. The diameter is easy to adjust by varying the number of zones so as to bring the in-focus intensity close to the ideal of the radiation intensity transmitted through the object [100].

4. Use of microparticles. The following experiment was proposed in [101]: placed in the path of a high-intensity X-ray FEL beam, 1 (Fig. 10b), is one biomolecule (the object) along

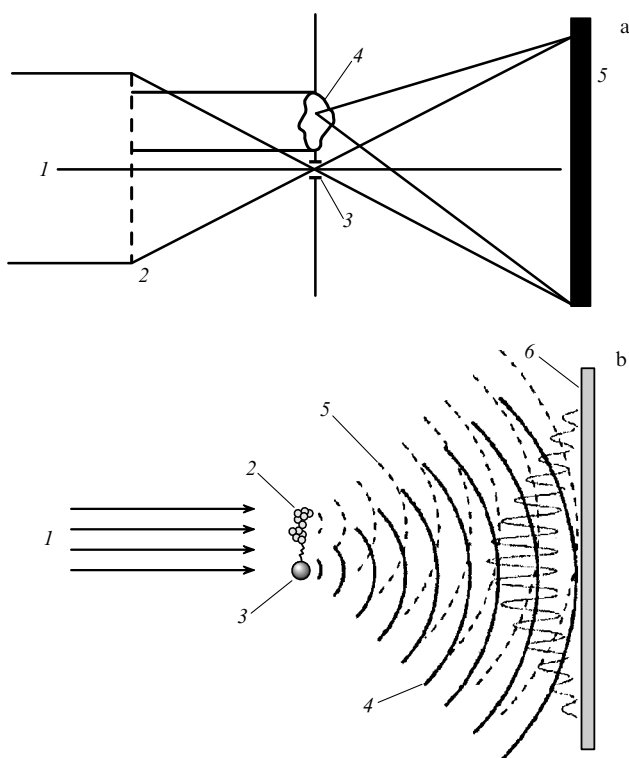


Figure 10. Fourier-transform holography schematics using (a) a Fresnel-zone plate and (b) microparticles [101] for the production of a reference wave. 1—primary beam. In Fig. 10a: 2—Fresnel zone plate, 3—order sorting aperture, 4—object, 5—detector. In Fig. 10b: 2—biomolecule (object), 3—nanodimensional gold particle, which is the source of a reference wave 4, 5—object wave, 6—detector.

with a small nanodimensional gold particle, 3, which is used as the source of a reference wave, 4. To provide a high intensity of the reference wave, a high- Z material must be used, because its scattering power is proportional to Z^2 .

The authors of Ref. [102] performed experimental tests of aerogel (silica) as a candidate for a standard point-like source of the reference wave. As discussed in that paper, although the aerogel works well as a reference, its scattering power is low due to the low density of the substance in use. The scattering power of the microparticle, which serves as the source of a reference wave, must be at least as high as the scattering power of the material of the sample under investigation.

An experiment on the holographic visualization of a diatom shell with a spatial resolution of 140 nm was reported in Ref. [103], which bore out the feasibility of realizing the idea stated in Ref. [101]. A small gold sphere served as the source of the reference wave in the experiment.

Fourier-transform holography was recently combined with iterative phase reconstruction methods to increase the resolution to the diffraction limit [79]. The combined approach involves recording a high-resolution X-ray hologram, and the holographic image obtained with the Fourier transform is next used as a starting point for iterative phase refinement [61, 62, 104, 105]. X-ray Fourier-transform holography is completely compatible with the iterative phase search if the hologram is recorded with a sufficiently high resolution. The uncertainties in the iterative procedure come to subtle details with a resolution below that of the holographic image. The resolution is ultimately limited not by

the reference size but by the largest X-ray photon momentum or the radiation wavelength.

Therefore, fast deterministic reconstruction and the possibility of attaining a high resolution make Fourier-transform holography an attractive visualization technique.

The progress of holography in the X-ray wavelength range is fostered primarily by the possibility of producing high-coherence high-intensity X-ray beams in modern third-generation synchrotrons [106] and by the progress of nanoscale fabrication. In particular, Fourier-transform holography was validly employed to visualize nanostructures owing to the polarization properties of SR. Sensitivity to magnetization, which arises from the effect of X-ray magnetic circular dichroism at $L_{2,3}$ absorption edges, was used for studying layered systems with perpendicular magnetic anisotropy, such as Co/Pt, [71, 73, 82] and Co/Pd [73, 81, 83, 107–110], as well as multilayer Co/Pt–Co/Ni–Co/Pt films [111]. The difference in image contrast of the holograms written with left- and right-polarized radiation yields purely magnetic information, which does not comprise nonmagnetic contributions caused, for instance, by variations in the sample thickness.

A new approach to overcoming the difficulties caused by the radiation damage to biological objects relies on the use of ultrashort FEL pulses [112]. The elegant idea consists in the measurement of the diffraction patterns of a series of biological samples (for instance, viruses or molecules) recorded under a single instance of illuminating each of them by a femtosecond pulse. An image recorded in the illumination of an object by a single pulse was demonstrated in Ref. [113]; also shown was the feasibility of performing experiments with temporal resolution. For the key step in obtaining ‘molecular films’, the authors of Ref. [84] proposed an approach involving division of the primary beam into two beams propagating along different optical channels: this approach permits recording two totally independent images with a variable femtosecond time delay. This concept overcomes the limitations imposed by the readout time of two-dimensional detectors, because two consecutive X-ray sample holograms can be obtained under single exposures and, nevertheless, they can be unambiguously separated in the reconstruction of two independent images.

The authors of Refs [114, 115] demonstrated a new approach to determining the 3D structure of nanodimensional crystalline materials using X-ray Fourier-transform holography in the Bragg geometry.

The instability of inversion algorithms in the presence of nonuniform deformation fields when Fourier-transform holography is used in the Laue geometry confines the method to several clearly defined systems, at least at present. Holography in the Bragg geometry, in the view of the authors of Ref. [115], is an attractive alternative to previous approaches owing to its capability to provide direct, reliable, and fast 3D reconstruction of the nanocrystal deformation density and field.

4. X-ray holography with an external radiation source and a detector (fluorescence holography)

It seems that the most promising line of the further development of X-ray structure analysis is the research on X-ray fluorescence holography (XFH), which has attracted the attention of many researchers as a new experimental tool for imaging the three-dimensional local atomic structure of crystals.

A distinction is made between direct and inverse methods of experimental XFH implementation, which are schematically shown in Fig. 11 [116, 117]. In the direct method [22–24, 118, 119], fluorescence diffraction pattern, 5 (Fig. 11a), results from the interference between the wave emitted by a point-like source (an atom), 3, and the waves singly scattered by the neighboring atoms, 2. This method is also referred to as ‘inner source’ holography. In the direct method, the hologram can be recorded while moving the detector over a large solid angle [120, 121].

The inverse approach [122] relies on the optical reciprocity principle, whereby the primary radiation source and the detector in the direct approach change places. One part of the X-ray beam, I , incident on the object (Fig. 11b), which does not interact with any of its atoms, serves as the reference beam. Another part scattered by the neighboring atoms, 2, which surround the selected detector atom, 3, is the object beam. The interference of these beams produces a spatially varying electromagnetic field, which results in the generation of fluorescence, 4, by the detector atom, with the intensity proportional to the squared amplitude of this field. Since the incident X-ray beam is perfectly collimated or covers only a small angular domain, the wave vector of the incident beam should scan the entire back space to produce a hologram. In this case, the recorded fluorescence intensity is equivalent to the hologram.

Gabor holography schemes do not reach atomic-scale resolution. One of the reasons (at least in the case of X-rays) is that the interference pattern is recorded only in a relatively small solid angle, i.e., with a small numerical aperture. Since the interference pattern in XFH is recorded in a solid angle that can range up to 4π , the resolution it provides can be of the order of the wavelength [123]. We emphasize once again that the fluorescent atom plays the role of a radiation source in the direct method and the role of a detector in the inverse one.

In considering the XFH features, we assumed the presence of only one fluorescent atom acting as a coherent wave source or as a detector of path length difference. In reality, there are many fluorescent atomic positions. However, if every emitter has the same environment, this fact poses no problem, because the reconstructed atomic image is a superposition of separate images.

We can see in Fig. 11 that the primary X-ray beam illuminates both the fluorescent atom and the atoms of its environment. This signifies that, in principle, it is possible to implement both hologram production modes described above. However, the experimental schemes of these modes are substantially different [124]. The angles φ and θ_2 are varied in the direct method (Fig. 12), and the position of the

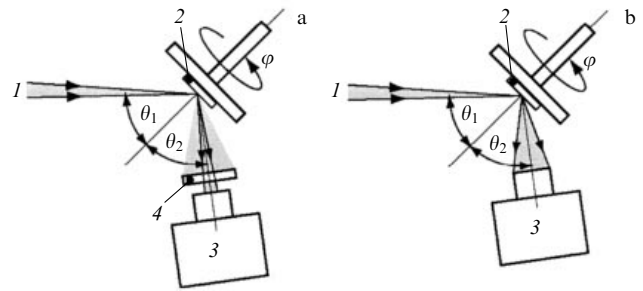


Figure 12. Experimental setups of (a) direct and (b) inverse XFH production modes: I —primary beam, 2—sample, 3—detector, 4—narrow slit in front of detector, θ_1 —angle of incidence of primary beam I , θ_2 —angle of reflection, φ —angle of rotation about the azimuthal axis.

primary beam is fixed ($\theta_1 = \text{const}$). In the inverse method, the angles φ and θ_1 are varied, and the position of the energy-dispersion detector, 3, remains invariable in the course of experiment. Nevertheless, the ‘raw’ experimental hologram is primarily a mixed hologram consisting of holograms generated in both the direct and inverse modes, and therefore it yields unreliable atomic images.

A purely inverse hologram can often be obtained with a detector located on the azimuthal axis of the sample, i.e., at $\theta_2 = 0$ [125], because in the rotation of the sample about the φ axis, the path difference between the reference and object waves does not change, leaving the ‘direct’ component invariable. Unfortunately, this ideal geometry is difficult to realize in practice: the holographic signal cannot be measured correctly in the rotation about the φ axis because the primary beam is blocked by the detector. In another method [126] for obtaining a purely inverse hologram, the detector and the sample are rotated synchronously. However, the implementation of this rotation requires a sophisticated experimental equipment. A purely direct hologram can be obtained when the primary beam is parallel to the φ axis, i.e., at $\theta_1 = 0$ [121]. But in this case, too, part of the information is lost due to the primary beam intersection by the detector.

A method for eliminating the ‘direct’ component from the inverse hologram was proposed in [126]. The authors showed that the direct component can be obtained by averaging experimental data over the angle θ_1 . However, the shape of this component turned out to be far from the expected sinusoid, and the component elimination procedure may give rise to errors in the image of the atomic structure. An experimental method for determining the ‘normal’ component was described in [127]. However, even a small inaccuracy

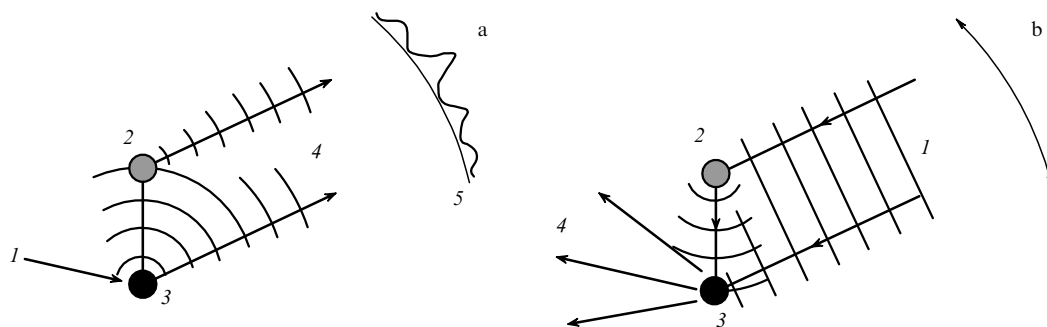


Figure 11. Schematics of (a) direct and (b) inverse methods for obtaining fluorescence holograms: I —primary beam, 2—ambient atom, 3—fluorescent atom, 4—fluorescence radiation, 5—hologram.

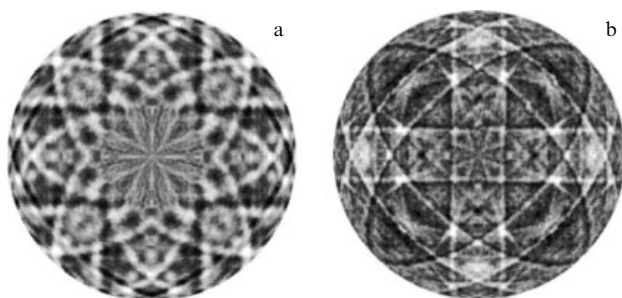


Figure 13. (a) Kossel lines and (b) XSWs in the holograms of an Au crystal, which were respectively obtained in the direct mode with the use of the AuL_{α} spectral line and in the inverse mode with the use of the primary MoK_{α_1} radiation of a laboratory radiation source [124].

in the alignment of the experimental equipment in the proposed method may result in significant errors. A practical method of subtracting the normal component from inverse XFH data by the Fourier transformation for a calculated hologram of a model ZnTe cluster was proposed in [128]. Clear atomic images were reconstructed at suitable positions of the model cluster using a mask function.

By the optical reciprocity theorem, the two XFH schemes described above are equivalent in many cases. Specifically, all experiments are performed on crystals, because the XFH requires objects with long-range rotational order and short-range translational order. Of all easily accessible solid-state objects, only crystals satisfy this requirement. For both XFH geometries, direct and inverse, the requirements for radiation coherence are practically insignificant (the spatial coherence should be of the order of interatomic distances).

In the investigation of crystal samples, features appear on holograms obtained in the direct or inverse modes, respectively interpreted as Kossel lines [129] or X-ray standing waves (XSWs) [130].

Kossel lines are formed when a point-like source is located inside the crystal: they are produced in the Bragg scattering of diverging X-rays by different crystallographic (lattice) planes.

In the case of XSWs, the source and detector change places relative to their location in the Kossel method (as noted in Refs [131, 132], the reciprocity theorem also holds in this case!); the atoms are subjected to a varying wave field in the crystal when the incident beam experiences Bragg reflection. As a result, in investigating crystals with long-range order, the use of the direct (inverse) method typically leads to Kossel lines (XSWs) in holograms (Fig. 13).

4.1 Multiple-energy fluorescence holography

But the main difference between direct and inverse XFH modes consists in the fact that the primary beam energy in the direct mode is limited by the excitation energy of fluorescence radiation. In the inverse mode, any energy exceeding the energy of the absorption edge of the chosen characteristic line series can be used, which is a significant advantage, as is to become clear in what follows [133].

In the reconstructed atomic images of a centrosymmetric crystal, an artifact (known as a double image problem) has been found, which may lead to quenching of the image of a specific atom [134]. To solve this problem, a multiple-energy XFH was proposed in [122]. In the inverse (direct) mode, the images reconstructed from holograms that were obtained for

different energies of primary (fluorescent) radiation by applying the multiple-energy Barton algorithm [135] are summed. In the summation, the phases participate additively in reconstructing the real atomic image and chaotically in reconstructing the imaginary one. Therefore, in the course of reconstruction, it is possible to extract the real atomic image, while its 'twin' vanishes owing to phase averaging. Its reliable elimination requires recording, as a rule, 5–10 holograms. This condition can be satisfied, for instance, with the use of SR. The inverse method allows obtaining a data set corresponding to different energies of the primary beam [136–139]. By contrast, by applying the direct method, it is only possible to record holograms with the use of no more than two to three characteristic spectral lines of the radiating atom (for instance, L_{α} , L_{β} , and L_{γ} [124]), and the reconstructed images may therefore be subject to the inevitable consequences of the overlap of real and imaginary object images as well as to undesirable aberrations and artifacts.

4.1.1 Experimental equipment. The main difficulty inherent in XFH is that the holographic signal is approximately three orders of magnitude weaker than the background signal of isotropic fluorescence. That is why the experiment requires a pure fluorescence signal and a detector with the highest possible count rate. However, such a detector has poor energy resolution, and a contribution to the holographic picture is made, apart from fluorescence radiation, by other elastically and inelastically scattered X-rays that emerge in Bragg diffraction as well as in diffuse and Compton scattering. Therefore, holographic measurements require that the experimental facility be equipped with an energy dispersion module. For such a module, an energy dispersion detector can be used, for instance, an avalanche photodiode (APD) [140] or a silicon drift detector (SDD) [141], or an analyzing crystal placed in front of the detector [142] (Fig. 14a). The main disadvantage of the former method is the limited dynamic range of existing energy dispersion detectors, while in the latter case, only a small solid acceptance angle is used.

One of the simplest ways of increasing the acceptance aperture may consist in the application of a sagittally focusing bent graphite analyzing crystal [25, 127, 143, 144]. It turns out, however, that preference should be given to the use of a cylindrical focusing analyzer made of LiF crystals [116, 145] or pyrolytic graphite [146–148]. Such an analyzer is depicted in Fig. 14b [148]. Four bent graphite crystals make up a hollow cylinder, which focuses fluorescence X-rays on the detector. The direct beam is stopped by a lead beam stop placed at the center of the analyzer. A more sophisticated toroidal graphite analyzer used in Refs [137, 149] furnishes a large acceptance angle, but it can be used for only one specific energy value.

To increase the X-ray photon intensity incident on the object, a focusing graphite monochromator [122, 124, 150, 151] or polycapillary optics [152] can be used.

4.1.2 Reconstruction of the object image. The majority of complications in holography emerge due to a low signal-to-noise ratio. Hence, all nonholographic signal constituents must be removed in the course of reconstruction. This applies, first and foremost, to Kossel lines (XSWs). Consequently, a prerequisite to obtaining good images is the removal of contributions to holographic intensity made by atoms that are not located in the immediate vicinity of the emitter

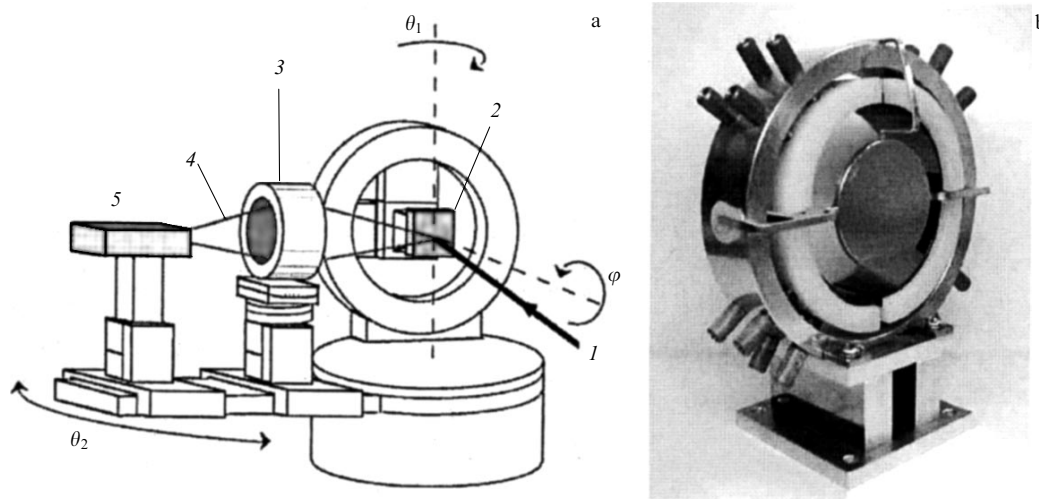


Figure 14. (a) Facility for performing experiments in fluorescence holography [145]: 1—primary beam, 2—sample mounted on a multi-circle goniometer, 3—cylindrical analyzer, 4—focused fluorescence radiation, 5—avalanche photodiode. (b) Exterior view of a four-sectional cylindrical graphite analyzer [148].

(detector). The solution to this problem given in 1991 by Tegze and Faigel [22] relies on the fact that different spatial frequency distributions of scattered radiation intensity are located at different distances from the emitter atom. It is evident that the high-frequency components originate from atoms that are far from the source and the low-frequency ones originate from atoms located close to the source. By applying a low-frequency filter, it is therefore possible to select the limit dividing surface around the atom serving as a source of fluorescence.

Low-frequency filtration limits the visibility range of atoms in the reconstructed image and suppresses high-frequency noise [153]. The applicability of this method was first demonstrated in numerical simulations [22] and subsequently in experiments [123, 127, 139, 154–158].

The XFH method requires that experimental data be recorded in broad angular and energy ranges. If a part of the data turns out to be damaged or missing due to experimental factors, the reconstruction procedure would yield invalid results throughout the real space, which may give rise to major artifacts or impairment of spatial resolution. This problem is inherent to all Fourier-transform methods. To avoid this problem, the solid angle of holographic data collection must be broadened to the entire sphere, which requires additional *a priori* information about the sample structure [127] and may be realized only for systems with a very high symmetry.

Owing to various circumstances (the features of the experimental facility, the shape and size of the object under investigation), scanning the object in the 4π space is not always possible. As a rule, the hologram ‘describes’ only a part of the entire sphere (Fig. 15a). However, to extend the data to the entire sphere, the symmetry can be used that follows from the crystal structure and is related to sharp intensity distribution singularities in the hologram corresponding to Kossel lines [127] or XSWs [136, 159].

Usually [116, 127, 139, 159], the processing of experimental data involves background subtraction from the normalized intensity variations in holograms, extension of the holographic data collection area to the entire sphere (Fig. 15b), low-frequency filtration (Fig. 15c), and the reconstruction of images corresponding to different energies

of the primary beam using the Helmholtz–Kirchhoff technique with application of the Barton transformation [135].

As shown in Ref. [127], it is possible to obtain images with a resolution close to the diffraction limit. But even in this case, the reconstructed wave field should be treated as a distorted image of the density distribution of scatterers. Despite the advantages of direct image reconstruction adopted as a simple Fourier transformation, the majority of problems require obtaining images of atomic arrangement in crystals with a resolution attainable only using iterative algorithms. The authors of Ref. [160] showed that iterative methods of deconvolution might be helpful in visualizing the atomic structure and improving the image quality, the greatest promise being shown by the maximum likelihood method.

Oscillating intensity pulsations about atomic images related to inaccuracies of the Fourier transformation in the Barton algorithm are quite often enhanced in reconstruction and are comparable to real images in intensity. Consequently, a new reconstruction algorithm apparently has to be developed in order to reconstruct the local structure of unknown samples with the use of multiple-energy XFH [161].

As shown in Refs [162, 163], using the scattering matrix technique in combination with the maximum entropy method instead of the commonly employed Barton algorithm allows reconstructing the local atomic structure more accurately. This approach was initially developed for photoelectron holography, but it is also helpful in XFH.

However, the reconstructed images may contain artifacts [164]. This is due to the long coherence length and mean free path of X-rays. As a result, the translational symmetry of a crystal was included in the maximum entropy algorithm. This inclusion is efficient and practically applicable, because there are many ways of measuring the translation vector. However, the translation algorithm cannot be applied when the local translational symmetry is broken around the emitter, for instance, under local deformations caused by impurities or adsorbents. But even with these drawbacks, the maximum entropy algorithm with the inclusion of translational symmetry is expected to become a powerful tool for determining atomic positions around specific atomic sites [164, 165].

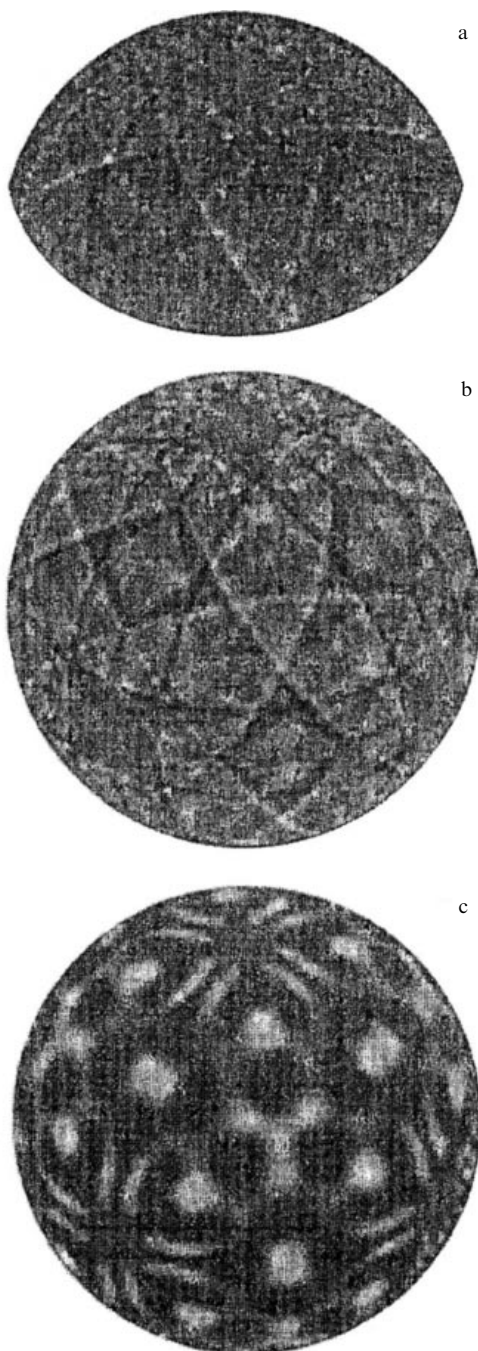


Figure 15. Au crystal hologram at different consecutive stages of processing. (a) 'Raw' hologram. (b) Hologram extended to a solid angle of 4π . (c) Hologram after low-frequency filtration [116].

4.1.3 Factors that affect image reconstruction. Primary beam energy. It was determined in [166] that the spatial resolution of atomic images increases with an increase in the incident beam energy, and the broader its energy variation range is, the lower the significance of aberrations and artifacts. Thus, when a hologram is recorded with a high-energy primary beam and a broad spectrum of several energies is used in a 4π solid angle, atomic images can be reconstructed from holograms with a high spatial resolution.

Sample absorption and shape. As already noted, all nonholographic signal constituents must be removed in the

course of image reconstruction. The largest contribution to unwanted signals is made by intensity modulation caused by the combination of two factors: the sample absorption and shape [24]. The simplest way of controlling absorption is to use samples with a flat surface. In this case, the angular dependence of intensity variation is determined analytically and can be readily calculated. The loss of information in the grazing geometry of primary beam incidence may be compensated with the inclusion of the symmetry of Kossel lines (XSWs).

Extinction effects. When a monochromatic primary beam is used, the X-ray absorption pattern may be 'smeared' by extinction effects resulting from multiple scattering in a crystal. This effect was profoundly analyzed in Ref. [167]. It was shown that the artifacts caused by extinction might also hinder the correct mapping of atomic positions in the holographic reconstructions in the investigation of imperfect crystals.

Polarization effect. As shown in Ref. [169], primary radiation polarization affects the quality of image reconstruction (either positively or negatively). SR is the most practical radiation source in the inverse XFH mode owing to its energy controllability, high brightness, and high spectral resolving power. But SR is linearly polarized, and this has to be taken into consideration. For instance, horizontally polarized SR suppresses holographic and reconstructed image intensities for atoms located in the horizontal plane of the radiation source and in so doing enhances the intensity for atoms located in the vertical plane [170].

Near-field effect. In the majority of early papers on XFH, an approximation was used where the size of the electron cloud was assumed to be much smaller than the curvature of the spherical wave front incident on the object, which was in fact true only for a point-like source. This approximation is incorrect when the scattering atom is located near the emitter atom. The image intensity in real space is reconstructed, as a rule, by applying the well-known Barton algorithm, in which the real density of the electron charge does not correspond to reality.

Apart from the simplest plane-wave scattering approximation, approaches can be used that take the curvature of the wave front into account. This problem was discussed in [171]. Three characteristic distances (length parameters) can be singled out: the radiation wavelength, the interatomic distance, and the size of the electron cloud. The ratio between them defines the magnitude of error caused by neglecting the curvature of the wave front. However, in the calculations in [171], the size of the electron cloud was not properly taken into account [172].

A formula for calculating the atomic scattering coefficient for spherical waves was derived in [173]; it was used in considering the near-field effect on fluorescence holography. The near-field effect due to wave front curvature becomes stronger as the X-ray radiation energy increases. This gives rise to phase shifts related to the size of the electron cloud. Taking the near-field effect into account, Tegze and Faigel [172] calculated the hologram of a spherical NiO cluster of more than 33,000 atoms and ascertained that its main 'feature' was its agreement with a hologram obtained experimentally.

4.2 Other methods of fluorescence holography

4.2.1 Two-energy method. Although multiple-energy XFH is a good method for suppressing the twin-image effect, obtaining

clear atomic images, as noted above, requires recording several (5–10) holograms and a long measurement time. As an alternative, the idea of a two-energy method was proposed in [174], which permits excluding the false image with the use of two holograms recorded with specially selected primary X-ray beam energies separated by several hundred electronvolts. The reconstruction algorithm implies that the phase of the conjugate image is certain to remain constant during reconstruction. The result of subtraction of the two images is therefore the removal of the false image.

The authors of Ref. [175] modified the proposed algorithm. Theoretical simulations suggested that the new algorithm was more efficient in operation than the Barton algorithm. Furthermore, it is quite likely that the majority of experiments presently performed on SR storage rings can be carried out on laboratory equipment with the use of the new two-energy algorithm [124, 150], since a tunable-energy source becomes optional and the measurements can be made using X-ray characteristic lines. This opens the way to the wide use of XFH in the near future.

4.2.2 Complex X-ray holography. Although the XFH technique in either of the two modes is a powerful tool for studying the local atomic structure around a given atom, it still does not incorporate the key feature of an ‘ideal’ probe: the method may be capable of identifying the reference (selected) atom but is not capable of identifying the neighboring atoms. The use of differences in the atomic scattering power is possible only when the atomic numbers of chemical elements are much different, as was shown for oxygen and nickel atoms in NiO crystals [139].

In 2002, to directly visualize the atoms of a preselected type, proceeding from theoretical simulations, resonance XFH was proposed [176], which permits reconstructing the atomic image of an element using differential holograms near the absorption edge. This new version of XFH is a unique method for determining the chemical environment of the reference atom and is an important improvement in multiple-energy XFH: it permits a direct determination of the ‘sort’ of the ambient atoms in reconstructed images even in complex cases, for instance, when the atomic numbers of the chemical elements are close.

Three energies E_1 , E_2 , E_3 are selected in resonance XFH that belong to a narrow energy range near the absorption edge E_{abs} of a neighboring atom: $E_1 < E_{\text{abs}}$, $E_2 = E_{\text{abs}}$, and

$E_3 > E_{\text{abs}}$. But a large variation of the scattering factor due to the resonance effect is observed only in the range of about 200 eV near the absorption edge. Considering that the multiple-energy XFH algorithm applicable here is efficient in the presence of a large number of holograms recorded in a range broader than 4 keV, the proposed method is subject to the twin-image effect. To solve this problem, a so-called complex XFH was proposed and elaborated in Refs [177–179].

In combination with resonance XR scattering, complex XFH permits reconstructing the environment of an atom of a selected chemical element in real space and solving the twin-image problem. For instance, in [177], to reconstruct the positions of Y atoms around an X atom, the primary beam energy can be taken to be near the YK absorption edge. Using the Y_{L_I} or $Y_{L_{II}}$ absorption edge and recording the $Y_{L_{\alpha}}$ fluorescence permit reconstructing the positions of Y atoms near a Y atom. Consequently, by selecting specific absorption edges, it is possible to determine the configurations of different kinds of atomic pairs, even in multicomponent systems. This allows investigating local atomic structures of more complex materials like high-temperature superconductors or magnetic materials.

4.2.3 X-ray absorption holography. This method is a version of the inverse method, in which the amplitude of a local wave field is indicated not by fluorescence radiation but by the absorption of wave fields in the sample.

The intensity $I(\mathbf{k})$ of radiation transmitted through a thin crystal plate, 2 (Fig. 16a), of a thickness t_0 illuminated by monochromatic radiation, I , of intensity I_0 has the form [180]

$$I(\mathbf{k}) \approx I_0 \exp(-\mu_0 t(\mathbf{k})) (1 - \mu_0 t(\mathbf{k}) \chi(\mathbf{k})), \quad (5)$$

where $\chi(\mathbf{k})$ is the normalized holographic intensity, $t(\mathbf{k}) = t_0 \cos \theta$, θ is the angle of incidence, and \mathbf{k} is the diffraction vector. As is evident from Eqn (5), the holographic signal is negative, and its ratio to the total measured signal increases by a factor of $\mu_0 t(\mathbf{k})$ in comparison with the similar ratio in the case of inverse XFH. X-ray absorption holography offers considerable advantages over inverse XFH [180]:

(1) the signal-to-background ratio can be increased by more than an order of magnitude by selecting the X-ray energy and/or the sample thickness. It is therefore possible to overcome one of the main drawbacks of atomic-resolution X-ray holograms — the weak scattering of hard X-rays;

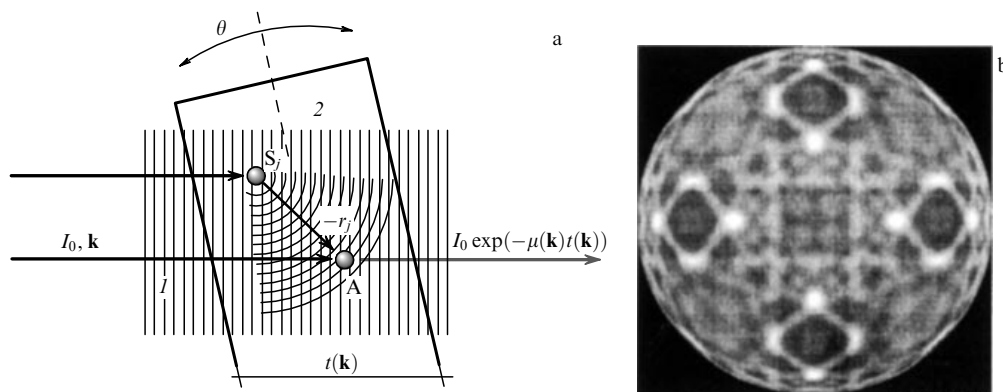


Figure 16. (a) Schematic of X-ray absorption holography: I —plane monochromatic wave, 2—sample, A—detector atom, S_j —ambient atom. (b) Absorption hologram of a thin CoO crystal; the primary beam energy is equal to 13 keV [180].

(2) the measured signal level is sufficient for performing experiments using not only high-power SR but also laboratory facilities equipped with conventional X-ray tubes;

(3) the elemental selectivity can be reached by taking the primary beam energy to be higher than the energy of the corresponding absorption edge. Nevertheless, X-ray absorption holography is capable of yielding helpful information about the structure of a sample that does not contain chemical elements with an absorption edge lying in the hard X-ray region;

(4) there is no need for energy discrimination of the X-rays detected, which significantly simplifies the experimental setup and data collection.

4.2.4 X-ray absorption anisotropy method. Korecki and Materlik [181] proposed an approach to X-ray holography for visualization in real space of the atomic structure around absorbing atoms in crystals, using a polychromatic X-ray beam for recording the absorption anisotropy pattern.

An increase in the spectral divergence $\Delta\lambda$ shortens the longitudinal coherence length $l_c = \lambda^2/\Delta\lambda$ and, consequently, makes the method ‘short-sighted’. From a practical standpoint, this signifies that a broadband spectrum ($\lambda/5 < \Delta\lambda < \lambda/2$) may be used to determine the directions of the bonds of the reference atom with the nearest neighbors, because the contribution of scattering of one atom is localized along the corresponding interatomic direction. A special feature of the method consists in a very short longitudinal coherence length of a ‘white’ X-ray beam (about 1 Å), which signifies that interference effects are noticeable only near the scattering direction, i.e., along the interatomic directions.

The features of the directional fine structure in the absorption of polychromatic X-ray radiation have a simple interpretation in real space. For ‘white’ X-rays, the wave field variations caused by the interference of the incident beam with the waves scattered by separate atoms decrease, on energy integration, in all directions except the direct scattering component coincident with the primary beam direction. As the sample orientation is varied, different atomic planes take the positions parallel to this direction, which changes the absorption of X-rays. Therefore, in the case of a crystal, it is possible to observe the projections of densely packed atomic planes.

These features of the method obviate the twin-image holographic problem, simplify the image reconstruction procedure (there is no need for a low-pass filtration), and

allow studying low-symmetry systems. Furthermore, a ‘white’ beam minimizes the so-called extinction effects, which make the data analysis in holographic methods cumbersome [167]. The absence of extinction effects for polychromatic radiation was experimentally demonstrated in Ref. [182].

The method of X-ray absorption anisotropy yields the averaged atomic structure around an absorbing atom inside the sample. Therefore, the absorption anisotropy may be recorded only for samples with rotational symmetry, i.e., for perfect and imperfect single crystals, multilayer structures, or samples with interfaces. However, quite often there are samples (consisting, for instance, of atoms of a single element) with a nonequivalent environment of the reference atom. In this case, the object image is a linear superposition of the patterns formed by nonequivalent structures. The method can be applied when the use of charged particles is impossible, for instance, in the imposition of an external electric or magnetic field on the sample.

The method of X-ray absorption anisotropy requires a broad and smooth X-ray spectrum. Any absorption edge within the energy range of the spectrum would give rise to sharp discontinuities and would complicate the data analysis. Another limitation of the method is a weak signal. However, recent experiments with the use of SR demonstrate interesting applications of the method. Preliminary results suggest that the method may also be implemented using laboratory equipment [152].

Initially, the X-ray absorption anisotropy in a white beam could be measured only using electron yields as a secondary emission [182]. However, the possibility of recording the absorption anisotropy using characteristic fluorescence radiation was demonstrated in Ref. [183].

The change from monochromatic to polychromatic radiation is attended by a qualitative alteration of the hologram character [181, 184]. The presence of a characteristic ‘shadow’ in the direction of primary radiation propagation becomes its main feature (Fig. 17). The ‘shadow effect’ allows directly observing the signal variation in the directions coinciding with the directions of dense atomic packing and with atomic planes [185].

Figure 18 shows the holographic pattern of X-ray absorption anisotropy for an InAs crystalline sample [186]. Its most conspicuous features are stripes that correspond to the projections of atomic planes.

A tomographic algorithm for the processing of polychromatic X-ray fluorescence holograms and 3D structure

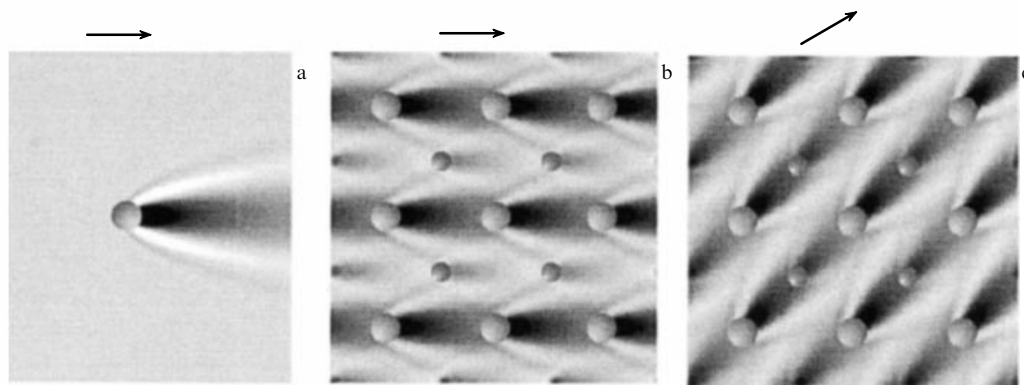


Figure 17. Spatial modulation of the X-ray wave field intensity with the use of ‘white’ X-ray radiation for (a) one atom and (b), (c) a crystal. Arrows indicate the primary beam direction.

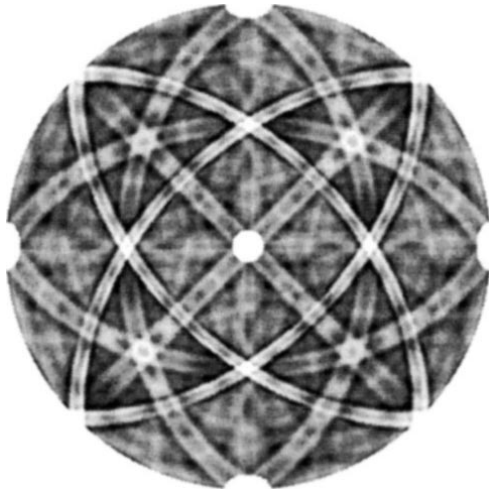


Figure 18. Holographic X-ray absorption anisotropy pattern for an InAs crystal with (001) surface orientation [186].

reconstruction was proposed in [187]. This algorithm, relying on the projective character of the polychromatic X-ray fluorescence holograms, involves measurements of the signal amplitude at the stripe center, where the projections are rather simple to interpret.

4.2.5 Bremsstrahlung X-ray holography. The nature of bremsstrahlung XFH is simple: when X-ray bremsstrahlung emerges inside a crystalline sample, the far-field intensity pattern becomes similar to a Gabor hologram [188]. The reference wave is formed by X-ray bremsstrahlung that arrives directly (without scattering) to the detector, and the object wave is formed by the X-ray bremsstrahlung scattered elastically by the atoms of an object in its path to the detector. The holographic pattern results from the interference of these waves in the detector plane. Simple Fourier analysis of this pattern can be used to reconstruct the images of atoms that surround the source atom [189].

Balanced Ross filters were used for the energy filtration of bremsstrahlung photons. This technique involves a combination of two filters fabricated of materials with slightly different atomic numbers. For elements with close atomic numbers, the energy dependences of their X-ray absorption coefficients are approximately the same, except in the region near their absorption edges. When the filter thickness is properly selected, the signal difference provides a narrow energy transmission band. The beam intensity transmitted first through one filter and then through the other is measured, and the difference between the two signals is then calculated.

Bremsstrahlung XFH is an attractive technique for three reasons: 1) materials with low atomic numbers are capable of producing short-wavelength radiation, which permits achieving a higher spatial resolution than with their characteristic low-energy radiation; 2) the bremsstrahlung cross section is high enough for recording holograms on laboratory equipment; 3) the bremsstrahlung spectrum is continuous, and it is therefore possible to simultaneously record several holograms corresponding to different X-ray photon energies, after which these holograms can be combined, as in the inverse XFH mode, for reconstructing the atomic object structure [189]. Numerical simulations have demonstrated the feasibility of bremsstrahlung X-ray holography.

However, there are practical difficulties in carrying out the method experimentally: a) because the bremsstrahlung is produced by electrons, the experiment must be carried out in the vacuum, the sample needs cooling (similar to the anode of an X-ray tube), and it must be a conductor; b) even if it is possible to provide a special medium that satisfies the previous requirement, the hologram would be formed by atoms of all sorts contained in the sample. The reason is that energy selection does not draw a distinction between atoms: any atom can be a source of X-rays of a given energy. This makes obtaining useful information difficult for multicomponent systems [24].

4.2.6 X-ray excited optical luminescence holography. In the inverse XFH mode, inner atomic electron shells are used as detectors. The possibility of employing outer electron shells for the study of crystalline objects exhibiting luminescence in the visible range was demonstrated in [190]. Holograms were obtained for ZnO-coated sapphire (Al_2O_3) in the recording of optical luminescence. The sample was irradiated by an X-ray beam with an energy of 15 keV. The positions occupied by Al and O atoms were reconstructed by the maximum entropy method [162, 163]. The processing of X-ray fluorescence holograms of samples containing light elements like Al or Si is usually difficult because of their small ionization cross sections and the absorption of their fluorescence radiation in the air. The resultant data suggest that hard X-rays can be used for reconstructing the positions of light elements in crystals with optical luminescence holography.

4.2.7 Gamma-ray holography. The idea of using ‘nuclear radiators’ in a crystal as internal detectors was expressed in Ref. [153]. A photon from an external gamma-ray source can be absorbed by a nucleus owing to a resonance process or can additionally be resonantly scattered. The interference of these two processes yields holographic variations of intensity measured as a function of the gamma-ray incidence angle [191]. Owing to the small nucleus size, the character of nuclear scattering is almost perfectly suited for holographic applications.

Gamma-ray holography is similar to the inverse XFH technique. But because a gamma-ray holographic experiment relies on the Mössbauer effect, it is possible to use only one wavelength, and multiple-energy holography seems unfeasible. Resonance scattering can nevertheless directly change the scattering phase by detuning from resonance [192], as in the case of resonance XFH discussed above. This detuning can be realized with the use of the Doppler effect by translating the sample at a certain velocity. Since holograms recorded near the Mössbauer resonance correspond to the same wavelength, they can be united into a hologram complex.

The idea proposed in Ref. [193] was to make the resultant hologram from a linear combination of two holograms recorded symmetrically below and above the exact resonance condition. The sum and difference of symmetrically recorded holograms always correspond to holograms with amplitudes of purely imaginary or purely real scattering. A complex gamma-ray hologram demonstrating the elimination of the twin-image effect was obtained in [193] for an epitaxial $^{57}\text{Fe}/\text{MgO}$ film, which confirms the potential of this method to become a useful tool for structural magnetic tomography [194].

Gamma-ray scattering is significantly different from electron scattering and X-ray scattering above the absorption edge. In gamma-ray holography, the characteristic features of nuclear resonance scattering are used. Since the cross section of nuclear resonance scattering is two orders of magnitude greater than the X-ray cross section, holographic experiments that employ nuclear scattering can be carried out with the use of laboratory equipment. The large cross section of nuclear resonance scattering may permit carrying out investigations of very thin films or highly diluted solid solutions enriched in resonance isotopes.

Another notable feature of nuclear resonance scattering is its sensitivity to hyperfine fields existing in solids, which permits distinguishing the positions of two similar atoms with different (nonequivalent) environments, i.e., studying magnetically ordered structures or structures containing atoms that differ only in valence [24]. Therefore, gamma-ray holography offers the advantage of high contrast and selectivity [195]. Nevertheless, it is limited by the number of special isotopes (Mössbauer nuclei). This limitation can be partly removed by using SR in combination with monochromators possessing a high energy resolution [196, 197].

4.3 Application of X-ray fluorescence holography

The use of SR in combination with high-resolution detectors permitted executing XFH-assisted measurements, which provided clear atomic images in a broad spatial range, up to the seventh coordination sphere [158]. Furthermore, XFH is highly sensitive to displacements of atoms from their ideal positions, and can therefore yield quantitative information about local lattice distortions at different spacing from the reference atom in the course of the analysis of reconstructed atomic images. In this subsection, we discuss examples of applying XFH (primarily its multiple-energy version) to investigations of a number of crystalline structures.

4.3.1 Impurities. The analysis of the atomic structure surrounding an impurity atom in a single crystal is one of the most important applications of XFH, capable of visualizing 3D distributions of local atomic structures in the range of several nanometers. This makes XFH a promising tool for estimating local lattice distortions around an impurity atom, which are closely related to the electronic material properties [198]. For instance, in [199], the three-dimensional image of the environment of Ga atoms was reconstructed in order to determine the degree of lattice distortions caused by the addition of Ga atoms to an InSb crystal. Although the atomic images are located at nearly perfect sites of the InSb crystal, some difference is observable for only the nearest-neighbor and second-nearest-neighbor atoms. From the XFH data, we can draw a conclusion that the lattice distortions of this semiconductor are limited to the range of the second coordination sphere.

In many papers, the emphasis is placed on the position of an impurity atom in the matrix lattice. For instance, it was determined that impurity zinc atoms in a GaAs crystal [156, 158, 200] and copper atoms (0.078%) in silicon steel [137] are in substitution positions and Er atoms in Sc_2O_3 reside in interstitial sites [201]. Investigations of a ZnSnAs_2 ferromagnetic semiconductor [202] and a Bi_2Te_3 topological insulator [203] with an Mn impurity showed that Mn atoms occupied the cation sites (those of Zn or Sn in the former compound and of Bi or Te in the latter one).

4.3.2 Crystalline films. Studies of impurity crystals in [137, 200] showed that the low density of fluorescent atoms does not limit the applicability of XFH. The majority of electronic devices are fabricated using the technology of epitaxial growth on single-crystal substrates. Because these film samples have translational order, the XFH technique should also be applicable to them, despite the small volume under irradiation. The feasibility of determining the local atomic structure of thin films was borne out by simulations of X-ray holograms of Ge atoms on a silicon substrate in a Ge film made of three atomic layers [168]. The potential of the method was experimentally demonstrated in the study of epitaxial films of different compositions and destinations: magnetic FePt [161, 204, 205], the semiconductor $\text{Si}_{0.8}\text{Ge}_{0.2}$ [117], superconducting $\text{EuBa}_2\text{Cu}_3\text{O}_{7-\delta}$ [149], and the DVD-RAM material $\text{Ge}_2\text{Sb}_2\text{Te}_5$ [206].

4.3.3 Mixed crystals. When a sample is not a perfect crystal, for instance, in the case of structural change on mixing with other elements, conventional diffraction techniques cannot yield precise atomic positions, because the perfect periodicity of the atomic structure is broken. The majority of functional materials are produced by mixing several chemical elements, and the resultant crystals are therefore imperfect. XFH is an ideal method for studying their atomic structure.

In [207], to investigate lattice distortions in a CdTe crystal with smaller ZnTe_4 tetrahedrons added as an impurity, the images of atoms surrounding the zinc atoms of a $\text{Cd}_{0.96}\text{Zn}_{0.04}\text{Te}$ mixed crystal were obtained in a wide spatial range with the use of ZnK_α X-ray fluorescence radiation. The lattice of this mixed crystal was shown to be distorted only within the first coordination sphere. This result is different from those obtained earlier in the investigation of the diluted magnetic semiconductors $\text{Zn}_{1-x}\text{Mn}_x\text{Te}$ [136, 208–210] and $\text{Cd}_{1-x}\text{Mn}_x\text{Te}$ [211] or an $\text{In}_{1-x}\text{Ga}_x\text{Sb}$ mixed crystal, in which lattice distortions extend to a distance of up to five chemical bonds.

In Ref. [213], measurements were performed on a thin $\text{Ge}_{0.6}\text{Mn}_{0.4}\text{Te}$ film under excitation by MnK_α fluorescence radiation. The data suggest that Ge atoms are replaced by Mn atoms in the GeTe matrix, and that the anion face-centered cubic (fcc) sublattice and Mn positions are stable. The reconstructed images suggest the instability of Ge positions or the existence of cation vacancies. To verify this inference, it was necessary to investigate the environment of Ge atoms. With the use of secondary GeK_α radiation, it was found in [214] that $\text{Ge}_{0.6}\text{Mn}_{0.4}\text{Te}$ has distortions around Ge atoms extending up to the third nearest neighbor. The distortion is associated with the instability of Ge positions. Even when the local structure around Ge atoms is strongly distorted, the environment of Mn atoms retains the O_h symmetry. Perhaps this is the reason why the $\text{Ge}_{0.6}\text{Mn}_{0.4}\text{Te}$ semiconductor has ferromagnetic properties [215].

4.3.4 Quasicrystals. An amazing property of quasicrystals is that although they are nonperiodic in the 3D space, their structure can nevertheless be characterized by a minimal set of parameters in the six-dimensional space similar to the real 3D space of 'normal' crystals. This 6D periodic structure can be projected on the 3D space to obtain an idealized quasicrystalline structure [216]. Proceeding from these models, it is possible to determine not only the long-range order but also the local order in different directions. To obtain the 3D atomic order pattern, it would be reasonable to attempt to

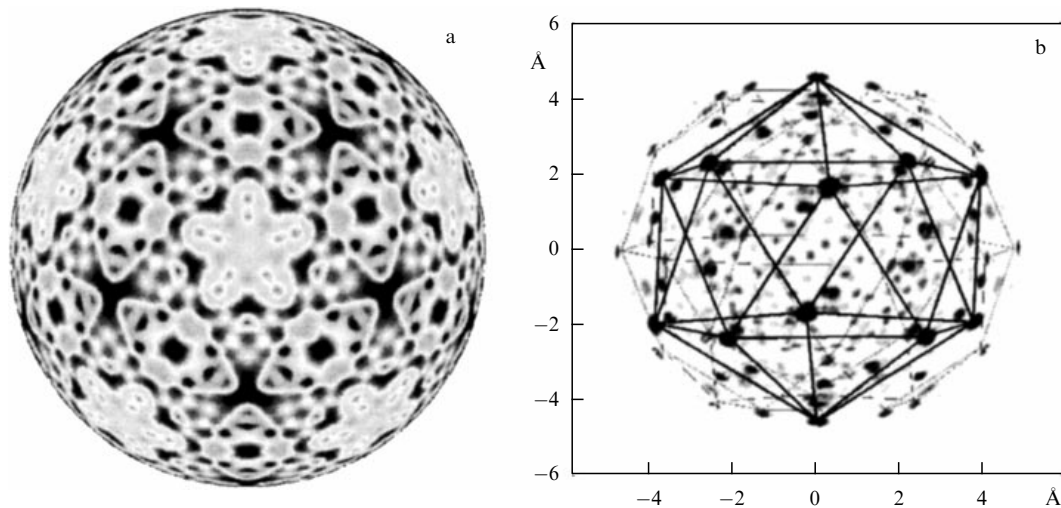


Figure 19. (a) Hologram of an $\text{Al}_{0.704}\text{Pd}_{0.21}\text{MnO}_{0.086}$ quasicrystal obtained for $E = 16$ keV upon low-frequency filtration, which demonstrates a five-fold noncrystallographic symmetry. (b) Reconstructed real-space environment of Mn atoms [217].

use traditional X-ray diffraction methods. In the majority of cases, however, the atomic structure of quasicrystals cannot be reconstructed this way. The use of holography allows obtaining the images of atoms surrounding, for instance, Mn atoms in an $\text{Al}_{0.704}\text{Pd}_{0.21}\text{MnO}_{0.086}$ quasicrystal (Fig. 19), as was done in Ref. [217].

The experiment in Ref. [217] opens the way to the application of atomic-resolution holography to studies of condensed media with orientation ordering, but without periodicity. Furthermore, XFH is an efficient method in the investigation of crystals with a high degree of mosaicity, which results in local variations of the orientation of the symmetry axis in solids. This provides a possibility of studying weakly ordered systems, for instance, proteins.

4.3.5 Alloys with shape memory. Phase transitions. Ti–Ni alloys are the most frequently used shape memory alloys; they exhibit a phase transition whose behavior depends on the amount of the third impurity element, Fe. A first-order phase transition is observed only when more than 6 weight percent of Fe atoms are replaced with Ni. Therefore, crystals of the composition $\text{Ti}_{0.50}\text{Ni}_{0.44}\text{Fe}_{0.06}$ are suitable samples for investigating structural modulation attended by the formation of a superlattice.

The local structure around Fe atoms in the $\text{Ti}_{0.50}\text{Ni}_{0.44}\text{Fe}_{0.06}$ alloy and its behavior under the phase transition were studied in Refs [218, 219] using XFH. The holograms were recorded with the use of FeK_α radiation at 225 and 100 K, which corresponds to the initial and commensurate phases. The atoms that are uniformly distributed in the initial phase form cluster structures with an 8 Å radius in the commensurate phase, in which the inter-cluster atomic motion is ‘frozen’. This information is valuable for explaining the phonon softening in the phase transition [198].

4.3.6 Ferroelectrics. An analysis of the reconstructed atomic images around Nb and Pb atoms in the ferroelectric relaxor $\text{Pb}(\text{Mg}_{1/3}\text{Nb}_{2/3})\text{O}_3$ (PMN) leads to a conclusion [220] that the PMN lattice consists of two sublattices. The first sublattice, which is formed by positionally stable Pb and Nb ions, constitutes pseudo-rhombohedral units built into a body-

centered elementary cell with a nonrhombohedral (perhaps orthorhombic) symmetry. The second sublattice consists of Pb and Nb ions vibrating around the ideal positions corresponding to a perovskite lattice. It may be assumed that the Pb and Nb ion vibrations are responsible for the characteristic relaxation spectrums observable in PMN.

The successful reconstruction of the complex $\text{Pb}(\text{Mg}_{1/3}\text{Nb}_{2/3})\text{O}_3$ crystal structure in Ref. [220] confirms the broad possibilities of atomic-resolution X-ray holography.

5. Conclusions

It is likely that X-ray holography is turning into a routine 3D visualization technique due to the improvement in spatial resolution, shortening of experiment time, and improvement in ways of reconstructing the sample images. Both methods — with an external and internal source/detector — complement each other well: the first enjoys application in investigations of amorphous or disordered (in particular, biological) objects, and the second permits determining the structure of ordered (crystalline) objects with atomic resolution.

The method with an internal source/detector (fluorescent holography method) has attracted considerable recent attention of researchers. Therefore, there is good reason to dwell on its advantages over the commonly used methods of investigating the structure of ordered objects like electron holography and transmission electron microscopy, X-ray diffraction (including the XSW method), the extended X-ray absorption fine structure technique, magnetic force microscopy, and Mössbauer spectroscopy.

1. As noted above, electrons are not an ideal means of visualization (especially holographic visualization) due to their strong interaction with substances and large phase shifts in scattering, while these effects are negligible for X-ray radiation. X-rays also have a higher penetration power than electrons do. Furthermore, electron-based methods require a vacuum, and the research object must exhibit conduction properties or be coated with a conducting film, which narrows the class of research objects and complicates experiments.

2. A distinguishing feature of X-ray holography is the simplicity of its experimental realization. X-ray microscopy requires precision focusing elements, necessitating a careful alignment of optical units, which complicates experiments.

3. Unlike diffractometry, holography does not require the existence of periodic long-range order; however, the structures surrounding the source atoms or detector atoms must be equivalent (and orientationally ordered). This signifies that holography permits studying structures that do not have perfect translation symmetry, e.g., imperfect crystals, macromolecules, hidden (internal) atomic layers, and deformed elementary cells.

4. The EXAFS technique is widely used to investigate the local atomic structure around a specific atom. However, this method can yield only 1D information. Furthermore, the information obtained with this method is usually limited to atoms of the second or third coordination spheres, unlike the information furnished by holography.

5. The method of magnetic force microscopy can be used to characterize the magnetic configuration of an object. But this method averages the results from all layers and does not permit studying each heterostructure layer separately. X-ray holography offers an advantage in sensitivity to a three-dimensional magnetization profile. Its specific feature consists in the capability to study complex magnetic heterostructure systems [90].

6. Although the data on object structure obtainable with γ -ray holography and Mössbauer spectroscopy are similar, their ranges of application are different: in γ -ray holography, the experimental scheme relies on the detection of Auger electrons, which can be used validly, for instance, to study superthin films [194].

It is noteworthy that apart from the advantages listed above, the main advantage of X-ray fluorescence holography is the capability of obtaining a three-dimensional image of the structure under investigation.

Further development of the methods using an external source (in-line holography and Fourier-transform holography methods) will most likely be related to FELs. The use of an FEL as a coherent X-ray source has attracted considerable interest of researchers [52, 80, 83, 84, 87, 93, 113, 114, 221].

A possibility has opened up to record fast dynamic processes at separate instants (phases): the use of femtosecond short pulses permits 'outrunning' the damage to the sample and obtaining atomic-scale structural information about the sample.

Furthermore, it is possible to dynamically visualize irreproducible ultrafast processes. Investigations of ultrafast phase transitions in mesoscopic systems, ultrafast spin inversions in magnetic nanodomains or major restructuring of molecules in biological media are some of the promising research subjects in the near future [93].

X-ray fluorescence holography is a unique method that not only is suitable for probing local structures at the medium range (several nanometers) but also is a candidate for many other structural characterizations yet to be developed. The structural information obtained with its aid establishes an efficient relation between routine X-ray diffraction methods for determining the long-range order in crystals and the EXAFS method.

Image reconstruction methods in electron and X-ray atomic-resolution holography were developed for small clusters. The existing hologram reconstruction algorithms are not always suitable for crystals, because they do not

always account for the medium field in a crystal caused by the rescattering of external electromagnetic field by all atoms of the crystal and, furthermore, do not take deformation fields into account. In some cases, the contribution to the image made by distant atoms is comparable in amplitude to the contribution from the nearest atoms and cannot be extracted without additional structural data about the object under investigation. In the view of the authors of Refs [222, 223], simple low-frequency filtration cannot be treated as a general method for complete elimination of the contribution that the scattering from distant atoms makes to the holographic dataset. Therefore, the widely used Barton reconstruction from filtered data may yield partially distorted information about atomic scattering amplitudes. This indicates the desirability of developing novel approaches and new algorithms.

Such approaches, unlike holographic reconstruction, which is an integral transformation, should ignore the data in the vicinity of Bragg diffraction. Perhaps other procedures of data analysis (for instance, with the use of the holographic analysis of structural factors [224] or a linear regression algorithm [225]) may hold greater promise. It is significant that, unlike holographic reconstruction, the indicated analysis procedures can be altered so as to include the physical effects disregarded by the kinematic theory: multiple scattering and extinction at angles close to the exact Bragg condition or fluorescence excitation away from this condition [152].

Therefore, although the physics of X-ray hologram formation is perfectly clear, the area of atomic-resolution holography still contains open questions. It is hoped that further theoretical and experimental research will facilitate correct unambiguous reconstruction of ordered structures of arbitrary complexity.

References

- Gabor D *Nature* **161** 777 (1948)
- Rogers G L *Proc. R. Soc. Edinburg A* **63** 193 (1952)
- Vander Lugt A *IEEE Trans. Inf. Theory* **10** 139 (1964)
- Leith E N, Upatniek J *J. Opt. Soc. Am.* **53** 1377 (1963)
- Stroke G W, Falconer D G *Phys. Lett.* **13** 306 (1964)
- Stroke G W *Appl. Phys. Lett.* **6** 201 (1965)
- Leith E N, Upatniek J, Haines K A *Phys. Rev.* **85** 763 (1952)
- Baez A V *J. Opt. Soc. Am.* **42** 756 (1952)
- Leith E N, Upatniek J, Haines K A *J. Opt. Soc. Am.* **55** 981 (1965)
- Winthrop J T, Worthington C R *Phys. Lett.* **15** 124 (1965)
- Winthrop J T, Worthington C R *Phys. Lett.* **21** 413 (1966)
- Stroke G W et al. *Br. J. Appl. Phys.* **17** 497 (1966)
- Rogers G L, Palmer J J *Microsc.* **89** 125 (1969)
- Aoki S, Kikuta S *Jpn. J. Appl. Phys.* **13** 1385 (1974)
- Reuter B, Mahr H J *Phys. E Sci. Instrum.* **9** 746 (1976)
- Kondratenko A M, Skrinisky A N *Opt. Spectrosc.* **42** 189 (1977); *Opt. Spektrosk.* **42** 338 (1977)
- Solem J C, Baldwin G C *Science* **218** 229 (1982)
- Szöke A *AIP Conf. Proc.* **147** 361 (1986)
- Saldin D K, de Andres P L *Phys. Rev. Lett.* **64** 1270 (1990)
- Harp G R, Saldin D K, Tonner B P *Phys. Rev. Lett.* **65** 1012 (1990)
- Len P M et al. *Phys. Rev. B* **59** 5857 (1999)
- Tegze M, Faigel G *Europhys. Lett.* **16** 41 (1991)
- Tegze M, Faigel G *Nature* **380** 49 (1996)
- Faigel G, Tegze M *Rep. Prog. Phys.* **62** 355 (1999)
- Faigel G, Tegze M G *Struct. Chem.* **14** 15 (2003)
- Faigel G et al. *X-Ray Spectrom.* **36** 3 (2007)
- Hayashi K *Adv. Imaging Electron Phys.* **140** 119 (2006)
- Hayashi K *e-J. Surf. Sci. Nanotechnol.* **9** 363 (2011)
- Hayashi K et al. *J. Phys. Condens. Matter* **24** 093201 (2012)
- Hosokawa S et al. *e-J. Surf. Sci. Nanotechnol.* **9** 265 (2011)
- McNulty I *Nucl. Instrum. Meth. Phys. Res. A* **347** 170 (1994)

32. Mandel L, Wolf E *Rev. Mod. Phys.* **37** 231 (1965)
33. Stoykova E, Kang H, Park J *Chin. Opt. Lett.* **12** 060013 (2014)
34. Xu W et al. *Appl. Opt.* **41** 5367 (2002)
35. Garcia-Sucerquia J et al. *Appl. Opt.* **45** 836 (2006)
36. Kreuzer H J, Pawlitzeck R A *Europhys. News* **34** (2) 62 (2003)
37. Gabor D *Proc. R. Soc. Lond. A* **197** 454 (1949)
38. Barton J J *Phys. Rev. Lett.* **61** 1356 (1988)
39. Kreuzer H J et al. *Ultramicroscopy* **45** 381 (1992)
40. Guigay J P *Optik* **49** 121 (1977)
41. Duhamel P, Vetterli M *Signal Processing* **19** 259 (1990)
42. Solem J C J. *Opt. Soc. Am. B* **3** 1551 (1986)
43. Soroko L M *Sov. Phys. Usp.* **9** 643 (1967); *Usp. Fiz. Nauk* **90** 3 (1966)
44. Latychevskaia T, Fink H-W *Phys. Rev. Lett.* **98** 233901 (2007)
45. Morlens A-S et al. *Opt. Lett.* **31** 3095 (2006)
46. Watanabe N et al. *Appl. Opt.* **36** 7433 (1997)
47. Watanabe N, Aoki S J. *Synchrotron Radiat.* **5** 1088 (1998)
48. Gorniak T et al. *Opt. Express* **19** 11059 (2011)
49. Heine R et al. *Ultramicroscopy* **111** 1131 (2011)
50. Lim J, Shin H J, Hong Ch K *Jpn. J. Appl. Phys.* **50** 072504 (2011)
51. Rosenhahn A et al. *Ultramicroscopy* **107** 1171 (2007)
52. Rosenhahn A et al. *Opt. Express* **17** 8220 (2009)
53. Barth R et al. *J. Biotechnol.* **149** 238 (2010)
54. Howells M et al. *Science* **238** 514 (1987)
55. Jacobsen C et al. *J. Opt. Soc. Am. A* **7** 1847 (1990)
56. Lindaas S et al. *J. Opt. Soc. Am. A* **13** 1788 (1996)
57. Wachulak P W et al. *J. Opt. Soc. Am. B* **25** 1811 (2008)
58. Kamijo N et al. *J. Synchrotron Rad.* **9** 182 (2002)
59. De Caro L et al. *Phys. Rev. B* **77** 081408(R) (2008)
60. Eisebitt S et al. *Phys. Rev. B* **68** 104419 (2003)
61. Gerchberg R W, Saxton W O A *Optik* **35** 227 (1972)
62. Fienup J R *Appl. Opt.* **21** 2758 (1982)
63. Rong L et al. *Opt. Lasers Eng.* **51** 553 (2013)
64. Kreuzer H J, Pawlitzeck R P, LEEPS, Version 1.2: a Software Package for the Simulation and Reconstruction of Low Energy Electron Point Source Images and Other Holograms (Halifax, NS: Helix Science Applications, 1993–1998)
65. Gabor D *Proc. IEEE* **60** 655 (1972); “Holography, 1948–1971. Nobel Lecture, December 13, 1971”, Preprint Les Pris Nobel en 1971 (Stockholm: The Nobel Foundation, 1972); Translated into Russian: *Usp. Fiz. Nauk* **109** 5 (1973)
66. Kohmura Y et al. *J. Appl. Phys.* **96** 1781 (2004)
67. Leith E N, Upatnieks J J. *Opt. Soc. Am.* **54** 1295 (1964)
68. Bonse U et al. *Nucl. Instrum. Meth.* **172** 223 (1980)
69. Lider V V *Phys. Usp.* **57** 1099 (2014); *Usp. Fiz. Nauk* **184** 1217 (2014)
70. Fuhse C, Ollinger C, Salditt T *Phys. Rev. Lett.* **97** 254801 (2006)
71. Eisebitt S et al. *Nature* **432** 885 (2004)
72. Eisebitt S et al. *Appl. Phys. Lett.* **84** 3373 (2004)
73. Hellwig O et al. *J. Appl. Phys.* **99** 08H307 (2006)
74. Guehrs E et al. *Opt. Express* **17** 6710 (2009)
75. Stickler D et al. *Appl. Phys. Lett.* **96** 042501 (2010)
76. Tieg C et al. *J. Phys. Conf. Ser.* **211** 012024 (2010)
77. Nomura K et al. *AIP Conf. Proc.* **1365** 277 (2011)
78. Schlotter W F et al. *Appl. Phys. Lett.* **89** 163112 (2006)
79. Stadler L-M et al. *Phys. Rev. Lett.* **100** 245503 (2008)
80. Kim H T et al. *Appl. Phys. Lett.* **98** 121105 (2011)
81. Spezzani C et al. *Phys. Rev. B* **88** 224420 (2013)
82. Streit-Nierobisch S et al. *J. Appl. Phys.* **106** 083909 (2009)
83. Wang T et al. *Phys. Rev. Lett.* **108** 267403 (2012)
84. Günther C M et al. *Nature Photon.* **5** 99 (2011)
85. Schlotter W F et al. *Opt. Lett.* **32** 3110 (2007)
86. Iwamoto H, Yagi N *J. Synchrotron Rad.* **18** 564 (2011)
87. Pfau B et al. *New J. Phys.* **12** 095006 (2010)
88. Podorov S G, Pavlov K M, Paganin D M *Opt. Express* **15** 9954 (2007)
89. Guizar-Sicairos M, Fienup J R *Opt. Express* **15** 17592 (2007)
90. Duckworth T A et al. *Opt. Express* **19** 16223 (2011)
91. Guizar-Sicairos M, Fienup J R *Opt. Lett.* **33** 2668 (2008)
92. Zhu D et al. *Phys. Rev. Lett.* **105** 043901 (2010)
93. Gauthier D et al. *Phys. Rev. Lett.* **105** 093901 (2010)
94. Marchesini S et al. *Nature Photon.* **2** 560 (2008)
95. Kondratenko A M, Skriniskii A N *Avtometriya* (2) 3 (1977)
96. McNulty I et al. *Science* **256** 1009 (1992)
97. Kirz J et al. *Phys. Scripta* (T31) 12 (1990)
98. Leitenberger W, Snigirev A J. *Appl. Phys.* **90** 538 (2001)
99. Malm E B et al. *Opt. Express* **21** 9959 (2013)
100. Geilhufe J et al. *Nature Commun.* **5** 3008 (2014)
101. Shintake T *Phys. Rev. E* **78** 041906 (2008)
102. Howells M R et al. *Nucl. Instrum. Meth. Phys. Res. A* **467** 864 (2001)
103. Guehrs E et al. *New J. Phys.* **14** 013022 (2012)
104. Fienup J R J. *Opt. Soc. Am. A* **4** 118 (1987)
105. Miao J et al. *Nature* **400** 342 (1999)
106. Kunz C J. *Phys. Condens. Matter* **13** 7499 (2001)
107. Hauet T et al. *Phys. Rev. B* **77** 184421 (2008)
108. Scherz A et al. *Phys. Rev. B* **76** 214410 (2007)
109. Günther C M et al. *Appl. Phys. Lett.* **93** 072505 (2008)
110. Günther C M et al. *Phys. Rev. B* **81** 064411 (2010)
111. Hellwig O et al. *Appl. Phys. Lett.* **98** 172503 (2011)
112. Mancuso A P et al. *New J. Phys.* **12** 035003 (2010)
113. Chapman H N et al. *Nature* **448** 676 (2007)
114. Chamard V et al. *Phys. Rev. Lett.* **104** 165501 (2010)
115. Roy S et al. *Nature Photon.* **5** 243 (2011)
116. Hayashi K, Takahashi Y, Matsubara E *Mater. Trans.* **43** 1464 (2002)
117. Hayashi K et al. *J. Mater. Sci. Mater. Electron.* **14** 459 (2003)
118. Faigel G et al. *Spectrochim. Acta B* **59** 1523 (2004)
119. Bompadre S G, Petersen T W, Sorensen L B *Phys. Rev. Lett.* **83** 2741 (1999)
120. Hayashi K et al. *Jpn. J. Appl. Phys.* **39** 1414 (2000)
121. Hiort T et al. *Phys. Rev. B* **61** R830 (2000)
122. Gog T et al. *Phys. Rev. Lett.* **76** 3132 (1996)
123. Adams B et al. *Phys. Rev. B* **57** 7526 (1998)
124. Takahashi Y, Hayashi K, Matsubara E *Adv. X-Ray Anal.* **47** 110 (2004)
125. Adams B, Nishino Y, Materlik G J. *Synchrotron Rad.* **7** 274 (2000)
126. Adams B et al. *Phys. Status Solidi B* **215** 757 (1999)
127. Tegze M et al. *Phys. Rev. Lett.* **82** 4847 (1999)
128. Happon N, Hayashi K, Hosokawa S *Jpn. J. Appl. Phys.* **49** 116601 (2010)
129. Lider V V *Crystallogr. Rep.* **56** 169 (2011); *Kristallografiya* **56** 195 (2011)
130. Zegenhagen J, Kazimirov A (Eds) *The X-ray Standing Wave Technique: Principles and Applications* (Series on Synchrotron Radiation Techniques, Vol. 7) (Singapore: World Scientific, 2013)
131. Gog T et al. *J. Physique IV C* **9** 449 (1994)
132. Gog T, Bahr D, Materlik G *Phys. Rev. B* **51** 6761(R) (1995)
133. Len P M et al. *Phys. Rev. B* **55** R3323 (1997)
134. Len P M et al. *Phys. Rev. B* **50** 11275(R) (1994)
135. Barton J J *Phys. Rev. Lett.* **67** 3106 (1991)
136. Hosokawa S, Happon N, Hayashi K *Phys. Rev. B* **80** 134123 (2009)
137. Hayashi K et al. *Nucl. Instrum. Meth. Phys. Res. B* **238** 192 (2005)
138. Mimura K et al. *e-J. Surf. Sci. Nanotechnol.* **9** 273 (2011)
139. Tegze M et al. *Nature* **407** 38 (2000)
140. Baron A Q R *Nucl. Instrum. Meth. Phys. Res. A* **352** 665 (1995)
141. Lechner P et al. *Nucl. Instrum. Meth. Phys. Res. A* **377** 346 (1996)
142. Sanchez del Rio M et al. *Proc. SPIE* **3448** 246 (1998)
143. Gog T et al. *Synchrotron Radiat. News* **9** 30 (1996)
144. Marchesini S, Belakhovsky M, Freund A K *Proc. SPIE* **3448** 224 (1998)
145. Hayashi K et al. *Nucl. Instrum. Meth. Phys. Res. A* **467–468** 1241 (2001)
146. Marchesini S et al. *Nucl. Instrum. Meth. Phys. Res. A* **457** 601 (2001)
147. Hosokawa S et al. *e-J. Surf. Sci. Nanotechnol.* **9** 265 (2011)
148. Takahashi Y, Hayashi K, Matsubara E *Sci. Technol. Adv. Mater.* **4** 409 (2003)
149. Sekioka T et al. *J. Synchrotron Radiat.* **12** 530 (2005)
150. Takahashi Y et al. *J. Mater. Res.* **18** 1471 (2003)
151. Gog T et al. *J. Electron Spectrosc. Relat. Phenom.* **92** 123 (1998)
152. Dabrowski K M, Korecki P *Nucl. Instrum. Meth. Phys. Res. B* **285** 94 (2012)
153. Tegze M *Phys. Rev. B* **73** 214104 (2006)
154. Takahashi Y, Hayashi K, Matsubara E *Powder Diffract.* **19** 77 (2004)
155. Faigel G, Tegze M, Bortel G *Phys. Rev. B* **70** 106101 (2004)
156. Hayashi K et al. *Anal. Sci.* **14** 987 (1998)
157. Busetto E et al. *Phys. Rev. B* **62** 5273 (2000)
158. Hayashi K et al. *Phys. Rev. B* **63** 041201 (2001)
159. Hu W et al. *J. Cryst. Growth* **311** 982 (2009)

160. Marchesini S, Fadley C S *Phys. Rev. B* **67** 024115 (2003)
161. Takahashi Y et al. *Appl. Phys. Lett.* **87** 234104 (2005)
162. Matsushita T, Agui A, Yoshigoe A *Europhys. Lett.* **65** 207 (2004)
163. Matsushita T, Yoshigoe A, Agui A *Europhys. Lett.* **71** 597 (2005)
164. Matsushita T et al. *Phys. Rev. B* **78** 144111 (2008)
165. Matsushita T et al. *e-J. Surf. Sci. Nanotechnol.* **9** 153 (2011)
166. Xie H et al. *Opt. Commun.* **229** 123 (2004)
167. Korecki P et al. *Phys. Rev. B* **69** 184103 (2004)
168. Takahashi Y, Hayashi K, Matsubara E *Mater. Trans.* **43** 1475 (2002)
169. Bortolani V, Celli V, Marvin A M *Phys. Rev. B* **67** 024102 (2003)
170. Len P M et al. *Phys. Rev. B* **56** 1529 (1997)
171. Adams B et al. *Phys. Rev. B* **57** 7526 (1998)
172. Tegze M, Faigel G J. *Phys. Condens. Matter* **13** 10613 (2001)
173. Bai J *Phys. Rev. B* **68** 144109 (2003)
174. Nishino Y et al. *Phys. Rev. B* **66** 092105 (2002)
175. Miao-Xin C, Zheng L *Chinese Phys. C* **32** 1016 (2008)
176. Omori S et al. *Phys. Rev. B* **65** 014106 (2001)
177. Takahashi Y, Hayashi K, Matsubara E *Phys. Rev. B* **68** 052103 (2003)
178. Takahashi Y, Hayashi K, Matsubara E *Phys. Rev. B* **69** 029902 (2004)
179. Takahashi Y, Hayashi K, Matsubara E *Phys. Rev. B* **71** 134107 (2005)
180. Kopecky M et al. *Phys. Rev. Lett.* **89** 279602 (2002)
181. Korecki P, Materlik G *Phys. Rev. Lett.* **86** 2333 (2001)
182. Korecki P et al. *Phys. Rev. Lett.* **96** 035502 (2006)
183. Korecki P et al. *J. Synchrotron Radiat.* **18** 851 (2011)
184. Korecki P, Tolkiehn M, Novikov D V *Radiat. Phys. Chem.* **78** S34 (2009)
185. Dabrowski K M et al. *Phys. Rev. B* **87** 064111 (2013)
186. Korecki P, Novikov D V, Tolkiehn M *Phys. Rev. B* **80** 014119 (2009)
187. Korecki P et al. *Phys. Rev. B* **74** 184116 (2006)
188. Miller G A, Sorensen L B *Phys. Rev. B* **56** 2399 (1997)
189. Bompadre S G, Petersen T W, Sorensen L B *Phys. Rev. Lett.* **83** 2741 (1999)
190. Hayashi K et al. *Phys. Rev. B* **76** 014119 (2007)
191. Korecki P, Korecki J, Ślōzak T *Phys. Rev. Lett.* **79** 3518 (1997)
192. Korecki P, Korecki J, Karaś W *Phys. Rev. B* **59** 6139 (1999)
193. Korecki P, Materlik G, Korecki J *Phys. Rev. Lett.* **86** 1534 (2001)
194. Korecki P, Korecki J *Hyperfine Interactions* **136–137** 137 (2001)
195. Korecki P et al. *Phys. Rev. Lett.* **92** 205501 (2004)
196. Burkel E *Rep. Prog. Phys.* **63** 171 (2000)
197. Toellner T S *Hyperfine Interactions* **125** 3 (2000)
198. Hayashi K, Happo N, Hosokawa S J. *Electron Spectrosc. Relat. Phenom.* **95** 337 (2014)
199. Hosokawa S et al. *Phys. Rev. B* **87** 094104 (2013)
200. Hayashi K et al. *Adv. X-Ray Anal.* **42** 181 (2000)
201. Anduleit K, Materlik G *Acta Cryst. A* **59** 138 (2003)
202. Hayashi K et al. *Jpn. J. Appl. Phys.* **50** 01BF05 (2011)
203. Hosokawa S et al. *J. Phys. Conf. Ser.* **502** 012024 (2014)
204. Takahashi Y et al. *Scripta Mater.* **48** 975 (2003)
205. Takahashi Y “Study of advanced x-ray fluorescence holography method”, PhD Thesis (Sendai, Japan: Tochoku Univ., 2004)
206. Hosokawa S et al. *Appl. Phys. Lett.* **90** 131913 (2007)
207. Happo N et al. *J. Electron Spectrosc. Relat. Phenom.* **181** 154 (2010)
208. Hosokawa S et al. *Jpn. J. Appl. Phys.* **44** 1011 (2005)
209. Happo N et al. *Inst. Pure Appl. Phys. Conf. Ser.* **7** 273 (2006)
210. Hosokawa S, Happo N, Hayashi K J. *Magn. Magn. Mater.* **310** 2707 (2007)
211. Happo N, Hayashi K, Hosokawa S J. *Cryst. Growth* **311** 990 (2009)
212. Hosokawa S et al. *J. Cryst. Growth* **311** 978 (2009)
213. Happo N et al. *Jpn. J. Appl. Phys.* **50** 05FC11 (2011)
214. Happo N et al. *e-J. Surf. Sci. Nanotechnol.* **9** 247 (2011)
215. Happo N et al. *J. Phys. Soc. Jpn.* **83** 113601 (2014)
216. Cahn J W J. *Res. Natl. Inst. Stand. Technol.* **106** 975 (2001)
217. Marchesini S et al. *Phys. Rev. Lett.* **85** 4723 (2000)
218. Hu W et al. *Phys. Rev. B* **80** 060202 (2009)
219. Hu W et al. *J. Cryst. Growth* **311** 982 (2009)
220. Hu W et al. *Phys. Rev. B* **89** 140103(R) (2014)
221. Martin A V et al. *Nature Commun.* **5** 4661 (2014)
222. Fanchenko S S et al. *Phys. Rev. B* **66** 060104(R) (2002)
223. Fanchenko S S et al. *Phys. Rev. B* **70** 106102 (2004)
224. Marchesini S et al. *Phys. Rev. B* **66** 094111 (2002)
225. Chukhovskii F N, Poliakov A M *Acta Cryst. A* **59** 109 (2003)